

The late-time radio behavior of GRB afterglows: testing the standard model

TUOMAS KANGAS¹ AND ANDREW S. FRUCHTER¹

¹*Space Telescope Science Institute
3700 San Martin Drive, Baltimore, MD 21218, USA*

(Received 2019; Revised 2020; Accepted 2021)

Submitted to ApJ

ABSTRACT

We examine a sample of 21 gamma-ray burst (GRB) afterglow light curves at radio frequencies, and compare them to the X-ray and/or optical properties of the afterglows and to the predictions of the standard jet/fireball model. Our sample includes every *Swift* GRB with an X-ray light curve indicating a jet break and with a published radio light curve, as well as several other targets with observed X-ray or and/optical jet breaks. We examine the late-time decline of each burst, and attempt to fit an analytical model based on the standard GRB afterglow equations to each data set. We show that most of the events in our *Swift* GRB sample are incompatible with the radio light curve behavior predicted by conventional afterglow theory. Many exhibit a late-time radio decline incompatible with the post-break X-ray or optical afterglow. Only one radio afterglow in this sample, at any time, shows the eventually expected decline of $\sim t^{-2}$, although two others show it in their mm light curve. Several others remain consistent with the standard model if such a decline began after the observations. The radio behavior alone does not, however, indicate whether a GRB can be fit by our modeling code. Indeed, several of the well-fit GRBs may only appear so due to a lack of multi-wavelength data. While a second source of emission can account for some of the anomalous radio behavior, our tests indicate this is often not the case unless the main jet component is simultaneously suppressed.

Keywords: gamma-ray burst: general — relativistic processes

1. INTRODUCTION

It is widely thought that the afterglow emission of a gamma-ray burst (GRB) originates as synchrotron radiation from electrons accelerated in the shock resulting from the interaction of the GRB jet with the circumburst medium (CBM; e.g. Paczynski & Rhoads 1993; Sari et al. 1998; Piran 2004). This standard fireball model predicts that the afterglow emission from X-ray to radio behaves as a series of (smoothly connected) power laws of the form $f_\nu \propto t^\alpha$, where the index α depends on the index of the electron energy distribution p and on the frequency in relation to the (evolving) breaks in the afterglow spectrum (e.g. Granot & Sari 2002). These break frequencies are the self-absorption frequency ν_a , the characteristic synchrotron frequency

ν_m and the cooling frequency ν_c . The relativistic nature of the jet and the resulting beaming of the emission from the jet is expected to cause an achronatic steepening of the light curve, known as a jet break, when the beaming angle becomes similar to the jet opening angle (Mészáros & Rees 1999; Rhoads 1999; Sari et al. 1999).

However, this model has not been able to explain all features of GRB afterglows. In particular, it has difficulty with what appears to be a population of radio quiet GRBs (Hancock et al. 2013; Lloyd-Ronning & Fryer 2017; Lloyd-Ronning et al. 2019). It was argued that these bursts (roughly a third of all GRBs) do not simply lack an observed radio afterglow due to insufficiently deep observations, but are indeed *intrinsically* radio-quiet. Lloyd-Ronning et al. (2019) further suggested that the two populations may have different progenitors: the radio-loud GRBs are typically longer and more luminous in γ -rays (especially at GeV energies where only radio-loud GRBs are detected), and

the radio-loud bursts alone show an anti-correlation between prompt duration and redshift. Active galactic nuclei (AGN) exhibit a similar radio-quiet vs. radio-loud dichotomy (Xu et al. 1999). Chiaberge & Marconi (2011) have suggested that radio-loud AGN require more massive and faster-spinning black holes than radio-quiet ones.

Another issue has been raised by several authors (Eichler & Waxman 2005; Giannios & Spitkovsky 2009; Ressler & Laskar 2017; Warren et al. 2018). A population of quasi-thermal electrons can exist in the jet in addition to the normally assumed power-law distribution, as the shock may only accelerate a fraction of the electrons (which may be as low as 0.01). The effect of this would be additional emission on top of the expected synchrotron spectrum – which should dominate in the radio while leaving higher frequencies largely unaffected (except in the hot electron model of Ressler & Laskar 2017). Meanwhile, ν_a would be increased by a factor of ~ 30 .

Yet another problem was presented by Kangas et al. (2020), hereafter referred to as K20. They analyzed the late afterglows of GRBs 160509A and 160625B between X-ray and radio, and found no post-jet-break decline in the radio light curve even a factor of 10 or 20 later than the observed optical/X-ray break. For GRB 160625B, in particular, the radio break was not observed even at ~ 200 days. Furthermore, the observed radio light curves were better described by a single power law ($\sim t^{-1}$) than by numerical afterglow models (van Eerten et al. 2012) in the decline phase. The only scenario permitted by the standard jet model (using equations from Rhoads 1999; Granot & Sari 2002) that produces a comparable behavior is a pre-break decline above ν_m .

A tendency of radio light curves of GRBs to be flatter than expected was noted earlier, in the pre-*Swift* era, by Frail et al. (2004), who noted that while the X-ray and optical slopes at late times were tightly correlated, radio and optical slopes were not. Some late-time radio light curves were even argued to flatten over time, which the authors explained with a transition to the non-relativistic phase. Frail et al. (2004) also brought up the possibility of changes in shock microphysics. Both they and K20 speculated that one possible solution might be a two-component jet where a wider, less energetic cocoon surrounds the core of the jet and would be responsible for the radio emission (suggested for GRB 030329 by Berger et al. 2003; Peng et al. 2005); see also Lazzati & Begelman (2005). Therefore radio emission from the ‘main’ component, commonly assumed to be the dominant source, may need to be suppressed somehow. Panaitescu & Kumar (2004) also included in their

sample some GRBs with jet breaks, where the effect of the jet break was not seen in the radio. Considering various explanations for decoupling optical and radio decay, they disfavored the two-component scenario and instead considered a semirelativistic reverse shock in a continuous inflow of ejecta more promising. Panaitescu (2005) examined a sample of GRBs through numerical modeling; a structured jet was able to improve the fit over the standard jet model for several bursts, but still did not fit the radio light curve well without severe scintillation effects, while delayed energy injection into a reverse shock was feasible for three bursts. Oates et al. (2007) noted that a two-component jet might resolve the discrepancy between X-ray and optical in GRB 050802, where a jet break was only seen in X-ray; while Uhm & Beloborodov (2007) suggested the reverse shock dominating *all* afterglow frequencies.

Based on the aforementioned studies, our understanding of the radio emission of GRB afterglows seems incomplete. In this paper, we follow up on the work of K20, attempting to shed more light on this picture by examining the radio light curves of 21 GRBs with an observed light curve break in the optical or X-ray. We compare the radio behavior to that of the higher frequencies, in particular concentrating on the radio decline rate, the presence or absence of an observed jet break, and the evolution of the peak frequency in the radio spectra. We show that most of the events in our sample, at radio frequencies, do not behave as expected after the X-ray jet break. We also attempt to fit each burst using the standard jet model; yet, in many cases a single power law is a better description of the radio decline. In Section 2 we present our sample and the methods we use to examine the properties of these GRBs through power-law fits and analytical modeling. Our results are presented in Section 3, and we discuss these findings in Section 4 and finally summarize our conclusions in Section 5. We adopt the notation $F_\nu \propto t^\alpha \nu^\beta$ for power-law light curves and spectra.

2. DATA AND ANALYSIS

2.1. The sample

The sample of GRBs we examine here was constructed as follows. In order to select only GRBs with probable jet breaks from the *Swift* X-Ray Telescope (XRT) GRB Catalogue¹, we picked each burst (as of January 2020) with at least one break in the X-ray light curve; where the last reported power-law slope is $\alpha_X < -1.5$; and where the change in the power law between the last and

¹ https://www.swift.ac.uk/xrt_live_cat/

GRB	z	$E_{\gamma, \text{iso}}$ (erg)	T_{90} (s)	Reference(s)
Group 1				
050820A	2.615	8.9×10^{52}	241 (<i>Swift</i> /BAT)	Cenko et al. (2006)
051022	0.8 ^a	4.4×10^{53}	≈ 200 (Konus- <i>Wind</i>)	Golenetskii et al. (2005); Rol et al. (2007)
070125	1.547	1.1×10^{54}	≈ 75 (Konus- <i>Wind</i>)	Golenetskii et al. (2007); Chandra et al. (2008)
090313	3.375	3.4×10^{52}	83 (<i>Swift</i> /BAT)	Melandri et al. (2010)
110709B	... ^b	...	810 (<i>Swift</i> /BAT)	Zauderer et al. (2013)
120326A	1.798	3.2×10^{52}	69 (<i>Swift</i> /BAT)	Laskar et al. (2015)
130907A	1.238	3.0×10^{54}	364 (<i>Swift</i> /BAT)	Veres et al. (2015)
141121A	1.469	8.0×10^{52}	≈ 1200 (Konus- <i>Wind</i>)	Golenetskii et al. (2014); Cucchiara et al. (2015)
151027A	0.81	4.0×10^{52}	130 (<i>Swift</i> /BAT)	Nappo et al. (2017)
160509A	1.17	8.6×10^{53}	371 (<i>Fermi</i> /GBM)	Roberts et al. (2016); Laskar et al. (2016); K20
160625B	1.406	3.0×10^{54}	460 (<i>Fermi</i> /GBM)	Burns (2016); Alexander et al. (2017); Troja et al. (2017); K20
171010A	0.33	2.2×10^{53}	104 (<i>Fermi</i> /GBM)	Poolakkil & Meegan (2017); Bright et al. (2019)
Group 2				
990510	1.62	2.9×10^{53}	68 (<i>BATSE</i>)	Kippen (1999); van Eerten et al. (2012) ^c
991208	0.706	1.2×10^{53}	68 (<i>Ulysses</i>)	Hurley et al. (2000b); Galama et al. (2000, 2003); Castro-Tirado et al. (2001)
000301C	2.04	5.4×10^{52}	≈ 10 (<i>Ulysses</i>)	Smith (2000); Berger et al. (2000); Sagar et al. (2000); Jensen et al. (2001); Rhoads & Fruchter (2001)
000926	2.08	2.6×10^{53}	≈ 25 (<i>Ulysses</i>)	Hurley et al. (2000a); Harrison et al. (2001); Price et al. (2001)
100418A	0.624	1.0×10^{51}	8 (<i>Swift</i> /BAT)	Moin et al. (2013); de Ugarte Postigo et al. (2018)
111215A	2.06 ^d	1.4×10^{53}	374 (<i>Swift</i> /BAT)	Zauderer et al. (2013); van der Horst et al. (2015)
140311A	4.954	1.0×10^{53}	70 (<i>Swift</i> /BAT)	Laskar et al. (2018a)
140903A	0.351	6.0×10^{49}	0.3 (<i>Swift</i> /BAT)	Troja et al. (2016)
161219B	0.148	1.8×10^{50}	7 (<i>Swift</i> /BAT)	Laskar et al. (2018b)

^aNo optical afterglow was detected, but the GRB was localized to a likely host galaxy at $z \approx 0.8$.

^bNo optical afterglow was detected. No E_{iso} available.

^cvan Eerten et al. (2012) compiled their data from Harrison et al. (1999); Israel et al. (1999); Bloom et al. (1999); Beuermann et al. (1999); Stanek et al. (1999), and Pietrzynski & Udalski (1999).

^dNo optical afterglow was detected – photometric host redshift given by van der Horst et al. (2015).

Table 1. GRB sample examined in this study. Group 1 refers to GRBs from our search of the entire *Swift* GRB Catalogue, and is thus considered representative; while Group 2 is the result of a literature search for additional GRBs and not necessarily representative.

second-to-last slope is $\Delta\alpha_X \leq -0.5$. These X-ray light curves were then visually inspected, and cases where the light curve behavior was clearly non-canonical until relatively late times (e.g. flaring activity with no clear power law segments), or where there were only a few X-ray data points, were removed. We then selected those bursts with published radio data in the literature. In the end, this left us with 12 GRBs. We refer to this subsample as Group 1.

In addition, we have included 9 other GRBs with published radio and X-ray/optical light curves and with a break in at least one frequency band that is consistent with a jet break (i.e. too steep to be the passage of ν_c). Events such as GRB 130427A (Perley et al. 2014; De Pasquale et al. 2016) with no observed jet breaks were

not included. In particular, we included those bursts examined by Panaitescu & Kumar (2004) with optical and/or X-ray light curves indicative of a jet break. This latter part of the sample, referred to as Group 2, is not necessarily a representative subsample of the full GRB population showing jet breaks, but is also included as additional examples of radio behavior.

Both subsamples and the main properties of the GRBs are summarized in Table 1. The duration, T_{90} , is obtained from the *Swift*/BAT GRB Catalog² unless otherwise specified. The sample includes a wide variety of GRBs including an ULGRB and a SGRB, three ‘dark’

² <https://swift.gsfc.nasa.gov/results/batgrbcatalog/>

GRBs with no detected optical afterglow, along with a broad range of redshifts ($0.1475 \leq z \leq 4.954$) and isotropic-equivalent energies ($6.0 \times 10^{49} \text{ erg} \leq E_{\gamma, \text{iso}} \leq 3.0 \times 10^{54} \text{ erg}$).

2.2. Power-law fitting

We have examined the radio and X-ray light curves of our sample of GRBs as follows. With the exception of GRBs 990510, 000926 and 140903A, the X-ray light curves were obtained from the *Swift*-XRT Lightcurve Repository³ and converted to flux densities at 5 keV using PIMMS⁴ and parameters from *Swift* (which in the case of GRB 130907A included a time-variable photon index). For the pre-*Swift*-era GRB 990510, X-ray fluxes were taken from [Kuulkers et al. \(2000\)](#) and converted to flux densities using the reported parameters. Fluxes of GRB 000926, also pre-*Swift*, were reported at 0.5 and 3 keV by [Harrison et al. \(2001\)](#). The late-time *Chandra* data associated with GRB 140903A were reported as flux densities at 1 keV; therefore we also convert the *Swift* X-ray data to 1 keV flux densities using parameters in [Troja et al. \(2016\)](#). Radio data were obtained from the sources listed in Table 1. The light curves at the fitted frequencies were in some cases augmented by interpolating between nearby frequencies, or by scaling to a nearby frequency assuming a power law spectrum ([Granot & Sari 2002](#)). We ignore any observed rise period of the light curve and any early features attributed to flares, plateaux or a reverse shock in the literature. To the light curve after these features (i.e. the decline only) we have attempted to fit a single power law of the form $f_\nu = f_{\nu,0} t^\alpha$ and a broken power law of the form

$$f_\nu = f_{\nu,0} \left[\left(\frac{t}{t_b} \right)^{-\omega\alpha_1} + \left(\frac{t}{t_b} \right)^{-\omega\alpha_2} \right]^{-\frac{1}{\omega}}, \quad (1)$$

where t_b is the break time (whether a true jet break or not) and ω is a parameter describing the sharpness of the break. We perform the fit using a fixed ω of 3 and 10 for each burst, and choose the fit with the smallest χ^2 (these were the values used by [Liang et al. 2007](#), and subsequently by K20). When a broken power-law fit is possible (i.e. at least five points to fit, as the function has four free parameters), we determine the presence or absence of a break in the light curve using an F-test for equality of variance between a single and a broken power law. We require an improvement at a $P_F > 0.95$ level, where P_F is the probability of a smaller difference in variance if the fits are equally good, to accept the break

as robust and at $P_F > 0.8$ to consider it ambiguous⁵. We use the fit to estimate p in the X-ray using standard closure relations; the break time t_j if applicable; and whether the break is consistent with the expected post-break slope of $\alpha_2 = -p$ from lateral expansion at the speed of sound ([Rhoads 1999](#)) or with a steepening by $t^{-3/4}$ or $t^{-1/2}$ depending on the density profile of the CBM ([Mészáros & Rees 1999](#); [Panaitescu & Mészáros 1999](#)). The latter, which we refer to as the edge effect, is only due to the edge of the jet becoming visible after an initial pseudo-isotropic phase, with no lateral expansion.

In the radio we have used the frequencies with enough points for a fit after any observed rising phase and/or early features in the light curve dominated by a reverse shock (seen in GRBs 050820A, 160509A, 160625B, and 161219B; [Cenko et al. 2006](#); [Laskar et al. 2016](#); [Alexander et al. 2017](#); [Laskar et al. 2018b](#)) – this means at least four points, so that we can better determine how well a power law fit matches the apparent decline. We make an exception in the case of GRB 140903A, where there are only three points available but they cleanly fit a single power law. Tables 2 and 3 list the results of our fits to Group 1 and 2 objects, respectively.

2.3. Analytical modeling

For each burst, we have also attempted to fit the standard afterglow model to the available data in order to check whether this model is able to reproduce the radio behavior. Even when no single (asymptotic) power-law segment predicted by the standard model matches the single or broken power-law fit, one can possibly obtain a good fit with a smooth transition from one slope to another, for example when break frequencies pass through the observed radio bands at certain times, and conversely, constraints imposed by other data may limit the applicability of the model even when the power law does seem compatible with it. We have developed a Python-based fitting code using the analytical representation of the evolution of a GRB synchrotron spectrum in [Granot & Sari \(2002\)](#) at times before the jet break and when there is no lateral expansion. After the jet break we have used the analytical model of [van der Horst \(2007\)](#) (their Table 2.10; based on [Rhoads 1999](#)) for the evolution of each break frequency and the normalization of the flux in the case of exponential lateral expansion. We also fit for the transition to non-relativistic expansion; the evolution of the break frequencies and normalizing flux in the non-relativistic phase is treated as described in Table 2.11 in [van der Horst \(2007\)](#).

³ http://www.swift.ac.uk/xrt_curves/

⁴ <http://cxc.harvard.edu/toolkit/pimms.jsp>

⁵ The notation P_F is used instead of the conventional p to avoid confusion with the index of the electron energy distribution p .

GRB	Band	Decline	t_{start}	α_1	α_2	t_b	Notes
050820A	5 keV	BPL	0.05 d	-1.14 ± 0.02	-1.68 ± 0.13	6.7 ± 1.8 d	...
	<i>r</i>	BPL	0.06 d	-0.87 ± 0.02	-1.66 ± 0.18	6.7 d	t_b fixed
	<i>i</i>	BPL	0.06 d	-0.86 ± 0.02	-1.69 ± 0.14	6.7 d	t_b fixed
	8.6 GHz	SPL	8 d	-0.66 ± 0.25
051022	5 keV	BPL	0.1 d	-1.42 ± 0.05	-2.50 ± 0.27	2.7 ± 0.6 d	Ambiguous break
	4.9 GHz	SPL?	1 d	-0.46 ± 0.17	Large scatter ^a
070125	5 keV	BPL	0.5 d	-0.71 ± 0.50	-2.00 ± 0.09	1.1 ± 0.3 d	Large α_1 error
	<i>r</i>	BPL	1 d	-0.05 ± 0.09	-1.88 ± 0.04	1.2 ± 0.1 d	...
	22.5 GHz	SPL	10 d	-0.58 ± 0.05
	14.9 GHz	SPL	10 d	-0.54 ± 0.23
	8.5 GHz	BPL?	17 d	-0.33 ± 0.11	-1.12 ± 0.32	88 ± 41 d	Ambiguous break
090313	4.9 GHz	SPL	27 d	-0.29 ± 0.06
	5 keV	BPL	0.3 d	-1.04 ± 0.14	-2.23 ± 0.17	1.0 ± 0.2 d	...
	<i>R</i>	SPL	0.015 d	-0.95 ± 0.04	Host-dominated after X-ray break
	<i>i</i>	SPL	0.01 d	-0.88 ± 0.03	Host-dominated after X-ray break
110709B	16 GHz	SPL	3 d	-0.31 ± 0.01
	5 keV	BPL	0.01 d	-0.91 ± 0.03	-1.57 ± 0.04	0.65 ± 0.06 d	...
120326A	5.8 GHz	SPL	6 d	-0.70 ± 0.10
	5 keV	BPL	0.5 d	-1.23 ± 0.19	-2.50 ± 0.26	1.4 ± 0.5 d	Ambiguous break
130907A	<i>r</i>	BPL	0.5 d	-0.95 ± 0.06	-2.52 ± 0.21	2.8 ± 0.3 d	Flattens at late times
	92.5 GHz	BPL?	Seems to break at $\lesssim 10$ d
	24.5 GHz	SPL	4 d	-0.87 ± 0.07
	19.2 GHz	BPL	4 d	-0.60 ± 0.07	-1.91 ± 0.99	44.7 ± 15.3 d	...
	5 GHz	BPL?	4 d	-0.43 ± 0.18	-1.23 ± 1.09	44.7 d ^b	Some scatter; ambiguous break
141121A	5 keV	BPL	0.01 d	-1.35 ± 0.02	-2.20 ± 0.03	0.25 ± 0.02 d	...
	15 GHz	SPL	0.5 d	-0.71 ± 0.04
	11 GHz	SPL	3 d	-0.88 ± 0.28	Some scatter
151027A	5 keV	BPL	0.5 d	-0.46 ± 0.11	-2.21 ± 0.19	3.8 ± 0.5 d	...
	15 GHz	SPL	3 d	-0.61 ± 0.08	Hints of the 7 GHz light curve shape
	7 GHz	SPL?	11 d	-0.45 ± 0.27	Not a clear SPL
	5 GHz	SPL?	6 d	0.19 ± 0.29	Not a clear SPL
	3 GHz	SPL?	16 d	0.88 ± 0.50	Not a clear SPL
160509A	5 keV	SPL	0.1 d	-1.65 ± 0.02
	<i>R</i>	BPL	0.05 d	-0.80 ± 0.29	-1.98 ± 0.13	0.5 ± 0.2 d	Flattens at late times
	5 GHz	BPL?	A hint of a break
160625B	5 keV	BPL	0.4 d	-1.20 ± 0.06	-1.96 ± 0.09	3.7 ± 0.8 d	...
	9 GHz	SPL	10 d	-0.92 ± 0.13
	6 GHz	SPL	10 d	-0.91 ± 0.11
171010A	5 keV	BPL	0.1 d	-1.24 ± 0.02	-2.23 ± 0.15	22 ± 4 d	...
	22 GHz	SPL	10 d	-0.75 ± 0.12
	6.1 GHz	SPL	20 d	-1.08 ± 0.11
171010A	5 keV	BPL	0.25 d	-1.29 ± 0.06	-1.98 ± 0.27	3.8 ± 1.6 d	...
	<i>R</i>	SPL	0.75 d	-1.13 ± 0.24	Flattens at late times; > 2.5 d ignored
	15.5 GHz	SPL	3 d	-1.12 ± 0.05

^aAttributed to scintillation by [Rol et al. \(2007\)](#).

^bFixed at the clearer break time of the 19.2 GHz light curve to make a BPL fit possible.

Table 2. Results of our single or broken power-law fits to the decline in the X-ray and radio light curves of Group 1 GRBs (and in the optical if it is relevant to the analysis), ignoring any rise in the light curve or features attributed to a reverse shock or late engine activity unless otherwise specified in the text; we thus only include points after t_{start} in the fit. In 'Decline', SPL corresponds to a single power law and BPL to a broken power law.

As the break frequencies ν_c , ν_m , and ν_a evolve differently with time, their order and thus the shape of the overall spectrum changes with time as well. [Granot & Sari \(2002\)](#) break the time evolution of the spectrum into five discrete regimes, determined by the order of the break frequencies. When one break frequency passes below another, the regime changes. Regime 1 corresponds to $\nu_a < \nu_m < \nu_c$, regime 2 to $\nu_m < \nu_a < \nu_c$, and regime 5 to $\nu_a < \nu_c < \nu_m$, in which case an additional absorption frequency, ν_{ac} , splits off from ν_a . The time evolution of ν_{ac} in the lateral expansion and non-relativistic cases,

not covered by [Granot & Sari \(2002\)](#) or [van der Horst \(2007\)](#), was determined for the sake of completeness using [Granot et al. \(2000\)](#); see Appendix A for details.

We assume a $5 \rightarrow 1 \rightarrow 2$ evolution over time. The evolution of these regimes is determined by Equations (1) – (9) of [Granot & Sari \(2002\)](#), while their Table 2 lists the parameters of each break frequency and the flux at that frequency in each regime. The break frequencies ν_a and ν_c are further affected by inverse Compton (IC) cooling. This lowers ν_c compared to the [Granot & Sari \(2002\)](#) predictions by a factor of $(1 + Y)^2$, where

GRB	Band	Decline	t_{start}	α_1	α_2	t_b	Notes
990510	5 keV	SPL	0.3 d	-1.43 ± 0.07
	V	BPL	0.1 d	-0.94 ± 0.01	-2.02 ± 0.03	1.3 ± 0.1 d	...
	i	BPL	0.6 d	-1.16 ± 0.04	-1.81 ± 0.05	1.4 ± 0.2 d	...
	8.6 GHz	SPL	3 d	-0.62 ± 0.10
991208	R	SPL	2 d	-2.41 ± 0.05	Jet break before observations
	I	SPL	2 d	-2.37 ± 0.25	Jet break before observations
	8.5 GHz	SPL	10 d	-1.00 ± 0.09
	1.4 GHz	SPL	7 d	-0.78 ± 0.18
000301C	B	BPL	1.5 d	-0.61 ± 0.07	-2.30 ± 0.17	3.8 ± 0.4 d	...
	R	BPL	1.7 d	-0.64 ± 0.05	-2.60 ± 0.10	4.6 ± 0.2 d	...
	K	BPL	1.7 d	-0.20 ± 0.05	-2.21 ± 0.09	3.6 ± 0.1 d	...
	8.5 GHz	SPL?	10 d	-0.74 ± 0.07	Hint of a break at ~ 100 d
	4.9 GHz	SPL	40 d	-1.73 ± 0.36	Large gap in light curve; possible break
000926	3 keV	SPL	2 d	-2.07 ± 0.47	Jet break before observations
	B	BPL	0.8 d	-1.22 ± 0.23	-2.26 ± 0.22	1.6 ± 0.3 d	...
	R	BPL	0.8 d	-1.64 ± 0.04	-2.28 ± 0.07	2.0 ± 0.3 d	...
	8.5 GHz	SPL	10 d	-0.68 ± 0.12
	4.9 GHz	SPL	10 d	-0.56 ± 0.10
100418A	5 keV	BPL	0.5 d	-1.01 ± 0.08	-1.85 ± 0.20	4.5 ± 1.2 d	...
	90 GHz	SPL	1 d	-0.60 ± 0.06
	8.5 GHz	SPL	38 d	-1.05 ± 0.21
	5.0 GHz	SPL	29 d	-0.41 ± 0.08
111215A	5 keV	SPL	0.1 d	-1.35 ± 0.03	May break at the same time as 93 GHz
	93 GHz	BPL	1 d	-0.20 ± 0.06	-1.73 ± 0.38	15 ± 3 d	Ambiguous break
	19.1 GHz	SPL	10 d	-1.08 ± 0.04
	6.7 GHz	SPL	15 d	-0.80 ± 0.09
	4.9 GHz	SPL	15 d	-0.56 ± 0.04
140311A	5 keV	BPL	0.1 d	-1.14 ± 0.11	-1.93 ± 0.48	1.3 ± 1.1 d	Ambiguous break
	24.5 GHz	SPL	4 d	-0.88 ± 0.07
	19.2 GHz	SPL	4 d	-0.80 ± 0.09
	13.5 GHz	SPL	4 d	-0.63 ± 0.12
	8.6 GHz	complex	Late-time rebrightening
140903A	1 keV	BPL	0.05 d	-0.95 ± 0.13	-2.31 ± 0.18	0.7 ± 0.2 d	...
	6.1 GHz	SPL	2 d	-0.64 ± 0.03
161219B	5 keV	BPL	0.05 d	-0.80 ± 0.01	-1.64 ± 0.11	17 ± 3 d	...
	r	SPL	0.08 d	-0.61 ± 0.01	SN-dominated points (> 2.7 d) ignored
	104 GHz	BPL	1 d	-0.48 ± 0.05	-1.47	...	Too few points for proper BPL fit
	11 GHz	SPL	15 d	-0.76 ± 0.02
	5 GHz	SPL	15 d	-0.63 ± 0.18

Table 3. As Table 2, but for Group 2.

Table 4. Upper and lower limits of each free parameter in our model fits.

Parameter	lower limit	upper limit
$E_{\text{K,iso}}$	10^{49} erg	10^{56} erg
p	2.0	3.2
n_0	10^{-5} cm $^{-3}$	10^4 cm $^{-3}$
A_*	10^{-5}	10^4
ϵ_e	10^{-5}	1
ϵ_B	10^{-6}	1
θ_0	0.01 rad	0.5 rad
A_V	0	5 mag

in regime 5, $Y \approx \sqrt{\epsilon_e/\epsilon_B}$ when $\epsilon_e \gg \epsilon_B$ (Sari & Esin 2001), thus prolonging regime 5. Simultaneously, ν_a is increased by a factor of $1 + Y$. After slow cooling begins at $t_{5 \rightarrow 1}$, the evolution of Y is approximated as a power law $Y \propto (t/t_{5 \rightarrow 1})^{(2-p)/(8-2p)}$ in the ISM case, and as $Y \propto (t/t_{5 \rightarrow 1})^{(2-p)/(4-p)}$ in the wind case, as per Equa-

tions (3.7) and (B1) in Sari & Esin (2001). We also include IC emission, as this can in some cases affect the X-ray light curve. Furthermore, we test each object for signs of Klein-Nishina suppression of the IC cooling described in (Nakar et al. 2009), using their Eq. 64; the process and its results are described in Appendix B.

To eliminate discontinuities in flux or break frequency across transitions from one spectral regime to another we use the following prescription. We compute the break frequencies and normalization flux of the spectrum from model parameters only at $t_{5 \rightarrow 1}$ calculated by equalizing ν_m and ν_c in regime 1, including the effect of IC cooling. Their evolution over time is then described with broken power laws, with each break corresponding to times of transition either from one regime to another; the jet break, with either lateral expansion (Rhoads 1999) or only the edge effect (Mészáros & Rees 1999; Panaitescu & Mészáros 1999); or a transition to the non-relativistic phase. Using an approach similar to that of Laskar et al.

(2014), the spectrum itself is computed as a sum of the spectra in each regime, weighted using a function w_i for regime i :

$$\begin{aligned} w_5 &= (1 + (t/t_{5 \rightarrow 1})^\eta)^{-1}, \\ w_1 &= (1 + (t/t_{5 \rightarrow 1})^{-\eta})^{-1} + (1 + (t/t_{1 \rightarrow 2})^\eta)^{-1} - 1, \\ w_2 &= (1 + (t/t_{1 \rightarrow 2})^{-\eta})^{-1}, \end{aligned} \quad (2)$$

where $t_{i \rightarrow j}$ is the transition time from i to j , and η is a sharpness parameter that we fix at 3. As each break in the spectrum is soft, the resulting light curve has no sharp breaks.

We have used the Markov chain Monte Carlo (MCMC) package EMCEE (Foreman-Mackey et al. 2013) to find the model parameters and their uncertainties through χ^2 minimization. The free parameters are p , isotropic-equivalent kinetic energy $E_{K,iso}$, the fractions of energy in electrons and magnetic fields ϵ_e and ϵ_B , the jet opening angle θ_j , and the density of the CBM n_0 (ISM) or A_* (wind). The optical, ultraviolet and infrared fluxes were corrected for Galactic reddening using the Schlafly & Finkbeiner (2011) dust maps and the Cardelli et al. (1989) extinction law; host galaxy extinction was corrected for using the Pei (1992) extinction law, with A_V as an additional free parameter in the fitting. For each parameter, we have used a simple top-hat prior (for parameters other than p and A_V , a logarithmic top hat) with upper and lower limits listed in Table 4. The jet break time t_j is determined by model parameters (van der Horst 2007):

$$\begin{aligned} t_{j,ISM} &= \frac{1+z}{2} \left(\frac{\theta_j}{0.126} \right)^{\frac{8}{3}} n_0^{-\frac{1}{3}} \left(\frac{E_{K,iso}}{10^{52} \text{ erg}} \right)^{\frac{1}{3}}, \\ t_{j,wind} &= \frac{1+z}{2} \left(\frac{\theta_j}{0.160} \right)^4 A_*^{-1} \left(\frac{E_{K,iso}}{10^{52} \text{ erg}} \right). \end{aligned} \quad (3)$$

At this point, the bulk Lorentz factor Γ is estimated as $\Gamma \approx \theta_j^{-1}$, and its evolution treated as a power law whose slope depends on the CBM profile and lateral expansion (Kumar & Zhang 2015): $\Gamma \propto t^{-1/2}$ with lateral expansion, $\Gamma \propto t^{-3/8}$ in an ISM-type CBM without lateral expansion or $\Gamma \propto t^{-1/4}$ in a wind-type CBM without lateral expansion. A good approximation of the transition to the non-relativistic phase is when $\Gamma \sim 1.3$ (Waxman et al. 1998), and we therefore place the transition there. We have separately run each fit with and without lateral expansion – as numerical simulations (e.g. Zhang & MacFadyen 2009; Granot & Piran 2012) suggest that exponential lateral expansion is not relevant for most afterglows – and with both constant-density and wind-type CBM for each target. Furthermore, we have run each of these with sharpness parameters 3 and 10 for the

jet break, as with the power law fitting. Out of these, the best fit is then shown; unless otherwise mentioned, this is simply the fit with the best χ^2 .

Points attributed to early reverse shock features, supernovae or host galaxy contamination in our source papers (Table 1) were discarded. A 15 per cent uncertainty floor was added to the data in all cases to avoid the fits being driven by a few exceptionally precise points. The luminosity distance of each object was obtained using the redshifts in Table 1 – with the exception of GRB 110709B, where the real redshift is unknown, so a fairly typical value of $z = 2.0$ was assumed⁶. We used the cosmological parameters in Bennett et al. (2014): $H_0 = 69.6 \text{ km s}^{-1} \text{ Mpc}^{-1}$; $\Omega_m = 0.286$; $\Omega_\Lambda = 0.714$. The best-fitting parameters and their uncertainties are listed in Table 5, along with the jet break time t_j , $\nu_m(t_j)$ and geometry-corrected energy E_K using the best-fit parameters.

3. RESULTS

Below, we describe the behavior of each individual GRB in our sample and whether some scenario of the conventional afterglow theory (Rhoads 1999; Granot & Sari 2002; van der Horst 2007) can account for all observations. For convenience, we summarize the scenarios and predicted light curve behavior in Table 6. In Figs. 1 through 21 we show the single or broken power-law fits and, if available, the best-fit analytical model (with the CBM and jet break types of the best fit), compared to the observed light curves of each individual object in our sample. We also show the radio spectral energy distributions (SEDs) of the objects where light curves at multiple (at least 3) radio frequencies are available, compared to best-fitting model spectra. In each light curve, the dashed vertical line corresponds to the jet break time in either the X-ray broken power law fit or our best-fit model. If data are available at enough frequencies to make the figure cluttered, we do not show all available frequencies; instead, we present a selection of frequencies that adequately demonstrates the behavior of the GRB compared to the model. All available data in our sources (Table 1) are used for model fitting, apart from any epochs specified below for each object and marked with open symbols, e.g. because of early reverse shock features or host galaxy contamination.

3.1. GRB 050820A

⁶ The assumed value of the redshift will change some of the fit values (see Zauderer et al. 2013), but for our purposes this is not relevant as long as one redshift results in compatibility with the standard model.

GRB	Model	$E_{K,iso}$ (10^{52} erg)	p	n_0 (cm^{-3}) or A_*	ϵ_e	ϵ_B	θ_j (rad)	A_V (mag)	Best-fit t_j (d)	$\nu_m(t_j)$ (Hz)	Best-fit E_K (10^{52} erg)
Group 1											
<i>050820A</i>	ISM/Edge	408^{+96}_{-63}	2.29 ± 0.03	$1.4^{+1.1}_{-0.3} \times 10^{-5}$	$0.06^{+0.02}_{-0.01}$	0.03 ± 0.02	0.027 ± 0.002	< 0.01	8.8	3.2×10^{11}	0.14
<i>051022</i>	Wind/Edge	$33.6^{+49.0}_{-16.0}$	$2.57^{+0.11}_{-0.12}$	$0.02^{+0.03}_{-0.01}$	0.13 ± 0.06	$0.03^{+0.11}_{-0.03}$	0.03 ± 0.01	...	1.6	1.1×10^{13}	0.16
<i>070125</i>	ISM/LE	$9.2^{+0.7}_{-0.4}$	$2.05^{+0.02}_{-0.01}$	$7.3^{+2.4}_{-1.1}$	0.35 ± 0.05	$0.43^{+0.12}_{-0.16}$	0.12 ± 0.01	$0.07^{+0.03}_{-0.02}$	0.25	3.6×10^{13}	0.06
<i>090313</i>	ISM/Edge	387^{+277}_{-377}	$2.04^{+0.22}_{-0.03}$	$0.90^{+0.24}_{-0.89}$	$0.04^{+0.06}_{-0.01}$	$0.014^{+0.005}_{-0.004}$	$0.04^{+0.09}_{-0.01}$	$0.27^{+0.14}_{-0.27}$	0.8	1.2×10^{11}	0.33
<i>110709B</i>	Wind/LE	$35.8^{+38.8}_{-12.6}$	$2.06^{+0.03}_{-0.02}$	$0.11^{+0.09}_{-0.05}$	$0.63^{+0.21}_{-0.20}$	$0.032^{+0.093}_{-0.028}$	0.04 ± 0.01	...	2.3	3.0×10^{12}	0.03
<i>120326A</i>	ISM/LE	$15.0^{+1.5}_{-1.2}$	2.05 ± 0.01	$0.40^{+0.07}_{-0.06}$	$0.83^{+0.04}_{-0.05}$	$0.15^{+0.05}_{-0.04}$	0.09 ± 0.01	0.35 ± 0.02	1.9	6.0×10^{12}	0.06
<i>130907A</i>	Wind/LE	441 ± 23	2.08 ± 0.01	0.03 ± 0.01	0.16 ± 0.01	$8.5^{+1.3}_{-1.1} \times 10^{-3}$	0.010 ± 0.001	1.3^b	0.25	1.8×10^{13}	0.02
<i>151027A</i>	Wind/LE	$72.1^{+21.3}_{-14.6}$	$2.91^{+0.07}_{-0.09}$	0.03 ± 0.01	$0.08^{+0.02}_{-0.01}$	$0.07^{+0.07}_{-0.04}$	0.04 ± 0.01	$1.1^{+0.1}_{-0.2}$	9.4	1.4×10^{10}	0.06
<i>160509A</i>	ISM/LE	$76.5^{+131.7}_{-34.4}$	$2.08^{+0.05}_{-0.03}$	$2.9^{+2.6}_{-1.6} \times 10^{-4}$	$0.53^{+0.27}_{-0.21}$	$0.012^{+0.060}_{-0.011}$	0.04 ± 0.01	$2.9^{+0.3}_{-0.4}$	3.1	1.6×10^{12}	0.06
<i>160625B</i>	ISM/Edge	194^{+31}_{-25}	2.38 ± 0.02	$1.1^{+0.2}_{-0.1} \times 10^{-5}$	0.16 ± 0.01	0.03 ± 0.01	0.041 ± 0.001	0.07 ± 0.02	15.8	8.6×10^{11}	0.16
<i>171010A</i>	ISM/LE	$10.5^{+3.1}_{-2.4}$	2.36 ± 0.03	$8.9^{+90.9}_{-0.7} \times 10^{-5}$	$0.06^{+0.05}_{-0.02}$	$0.32^{+0.38}_{-0.28}$	$0.06^{+0.03}_{-0.01}$	$0.02^{+0.04}_{-0.02}$	4.0	4.2×10^{11}	0.02
Group 2											
<i>990510</i>	Wind/LE	$28.7^{+126.7}_{-10.7}$	$2.07^{+0.13}_{-0.03}$	$0.06^{+0.10}_{-0.03}$	$0.31^{+0.16}_{-0.11}$	$0.03^{+0.12}_{-0.03}$	0.04 ± 0.01	< 0.01	1.6	1.6×10^{12}	0.02
<i>991208</i>	Wind/LE	2.2 ± 0.5	$2.09^{+0.02}_{-0.01}$	0.56 ± 0.07	$0.83^{+0.08}_{-0.10}$	$0.06^{+0.03}_{-0.02}$	$0.12^{+0.02}_{-0.01}$	< 0.01	1.2	9.1×10^{12}	0.02
<i>000301C</i>	ISM/LE	$88.9^{+209.5}_{-69.6}$	$2.68^{+0.05}_{-0.08}$	$1.4^{+0.9}_{-1.0}$	$0.26^{+0.13}_{-0.12}$	$7.4^{+39.5}_{-7.0} \times 10^{-5}$	0.13 ± 0.02	< 0.01	6.2	7.3×10^{11}	0.72
<i>000926</i>	ISM/Edge	$27.5^{+5.0}_{-16.7}$	$2.27^{+0.07}_{-0.08}$	$36.2^{+3.8}_{-34.7}$	$0.29^{+0.06}_{-0.18}$	$7.1^{+128.9}_{-1.9} \times 10^{-4}$	$0.11^{+0.01}_{-0.02}$	$0.10^{+0.08}_{-0.02}$	1.0	5.5×10^{12}	0.16
<i>100418A</i>	ISM/Edge	$0.36^{+0.11}_{-0.03}$	$2.26^{+0.03}_{-0.02}$	$0.08^{+0.03}_{-0.02}$	0.38 ± 0.03	$0.47^{+0.12}_{-0.26}$	0.45 ± 0.02	$0.39^{+0.04}_{-0.03}$	38.6	8.3×10^{10}	0.03
<i>111215A</i>	Wind/LE	770^{+201}_{-159}	$2.92^{+0.05}_{-0.08}$	0.20 ± 0.03	$0.12^{+0.01}_{-0.02}$	$5.4^{+4.0}_{-1.8} \times 10^{-3}$	0.03 ± 0.01	...	10.8	2.8×10^{12}	0.43
<i>140311A</i>	ISM/LE	2270^{+1380}_{-1860}	$2.21^{+0.18}_{-0.08}$	$1.13^{+0.80}_{-1.06}$	$0.37^{+0.18}_{-0.23}$	$4.7^{+249.1}_{-3.2} \times 10^{-6}$	$0.03^{+0.03}_{-0.01}$	$0.69^{+0.03}_{-0.08}$	1.2	4.3×10^{12}	1.34
<i>140903A</i>	ISM/LE	$47.3^{+244.0}_{-37.1}$	$2.46^{+0.03}_{-0.08}$	$3.5^{+246.8}_{-3.3} \times 10^{-4}$	$0.09^{+0.07}_{-0.05}$	$1.57^{+48.27}_{-1.53} \times 10^{-4}$	$0.03^{+0.03}_{-0.02}$	$0.36^{+0.05}_{-0.11}$	1.1	4.1×10^{11}	0.03

^aFor dark GRBs (GRBs 051022, 110709B and 111215A), optical extinction is not relevant and was fixed at zero.

^bFor GRB 130907A, extinction was fixed at $A_V = 1.3$ as per Veres et al. (2015) (see text).

Table 5. MCMC fit parameters and their uncertainties for each GRB in our sample. Both types of CBM (ISM and wind) and both types of jet break, with exponential lateral expansion (abbreviated as 'LE') and without it ('Edge'), were attempted for each burst, and the listed model is the best-fitting of these four. We note that in many cases, the best wind and ISM fits have roughly equal χ^2 . Names of GRBs that we consider consistent with the model are italicized.

Frequency sequence	Pre-break		Edge effect		Lateral expansion	Non-relativistic	
	$k = 0$	$k = 2$	$k = 0$	$k = 2$		$k = 0$	$k = 2$
$\nu < \nu_{ac} < \nu_a < \nu_c < \nu_m$	1/2	1	-1/4	1/2	0	7/8	-121/72
$\nu_{ac} < \nu < \nu_a < \nu_c < \nu_m$	11/16	1	-1/16	1/2	1/4	7/8	-133/72
$\nu_{ac}, \nu_a < \nu < \nu_c < \nu_m$	1/6	-2/3	-7/12	-7/6	-1	2/3	-2/3
$\nu_{ac}, \nu_a < \nu_c < \nu < \nu_m$	-1/4	-1/4	-1	-3/4	-1	1/2	1/6
$\nu_{ac}, \nu_a < \nu_c < \nu_m < \nu$	$-\frac{3p-2}{4}$	$-\frac{3p-2}{4}$	$-\frac{3p+1}{4}$	$-\frac{3p}{4}$	$-p$	$-\frac{3p-4}{2}$	$-\frac{7p-8}{6}$
$\nu < \nu_a < \nu_m < \nu_c$	1/2	1	-1/4	1/2	0	-2/5	2/3
$\nu_a < \nu < \nu_m < \nu_c$	1/2	0	-1/4	-1/2	-1/3	8/5	4/9
$\nu_a < \nu_m < \nu < \nu_c$	$-\frac{3(p-1)}{4}$	$-\frac{3p-1}{4}$	$-\frac{3p}{4}$	$-\frac{3p+1}{4}$	$-p$	$-\frac{3(5p-7)}{10}$	$-\frac{7p-5}{6}$
$\nu_a < \nu_m < \nu_c < \nu$	$-\frac{3p-2}{4}$	$-\frac{3p-2}{4}$	$-\frac{3p+1}{4}$	$-\frac{3p}{4}$	$-p$	$-\frac{3p-4}{2}$	$-\frac{7p-8}{6}$
$\nu < \nu_m < \nu_a < \nu_c$	1/2	1	-1/4	1/2	0	-2/5	2/3
$\nu_m < \nu < \nu_a < \nu_c$	5/4	7/4	1/2	5/4	1	11/10	11/6
$\nu_m < \nu_a < \nu < \nu_c$	$-\frac{3(p-1)}{4}$	$-\frac{3p-1}{4}$	$-\frac{3p}{4}$	$-\frac{3p+1}{4}$	$-p$	$-\frac{3(5p-7)}{10}$	$-\frac{7p-5}{6}$
$\nu_m < \nu_a < \nu_c < \nu$	$-\frac{3p-2}{4}$	$-\frac{3p-2}{4}$	$-\frac{3p+1}{4}$	$-\frac{3p}{4}$	$-p$	$-\frac{3p-4}{2}$	$-\frac{7p-8}{6}$

Table 6. Standard model predictions of the indices of power law segments in afterglow light curves. The values have been compiled using formulae in Granot et al. (2000), Granot & Sari (2002) and van der Horst (2007); the edge effect values are the pre-break slopes plus a steepening by $t^{-3/4}$ or $t^{-1/2}$ when $k = 0$ and $k = 2$, respectively.

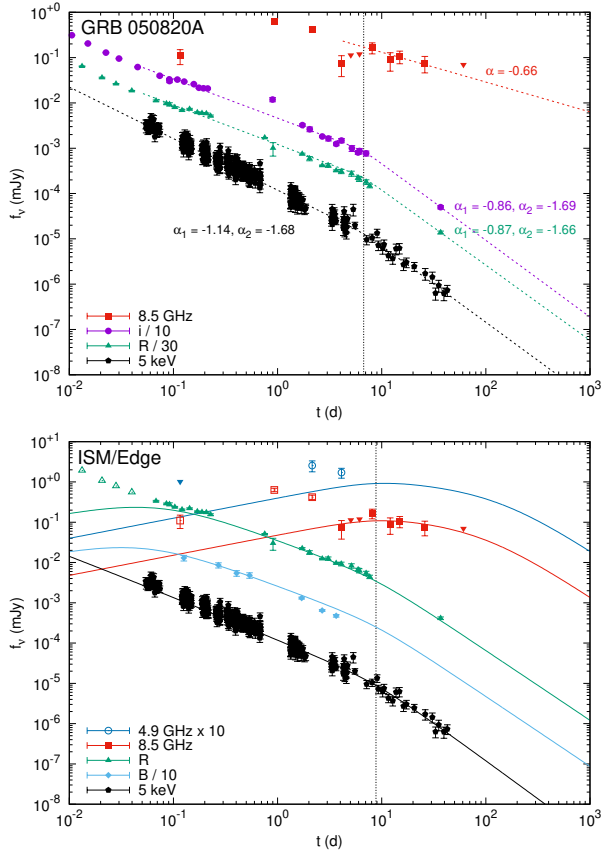


Figure 1. Our single and broken power law fits (upper panel) and best-fitting analytical model (lower panel) compared to the light curves of GRB 050820A. Three additional optical frequencies used in the fitting are omitted from this figure for clarity.

The X-ray light curve is consistent with an edge effect jet break in wind-type CBM (the observed $\Delta\alpha = -0.54 \pm 0.14$); this in turn implies $p \approx 2.2$. In an ISM scenario with the edge effect, the expected $\Delta\alpha = -3/4$ is $\sim 1.6\sigma$ from the observed value. The optical decay is consistent with $p \approx 2.2$ as well, but only in an ISM-type CBM and when $\nu_a, \nu_m < r, i < \nu_c < 5$ keV, as the X-ray decline at < 10 d is steeper than the optical by $t^{0.27 \pm 0.03}$. Cenko et al. (2006) argued that the radio light curve includes a reverse shock before ~ 4 d, although a reverse shock model was not explored in detail. The radio decay after this point can be fitted with a single power law; the slope of this power law is consistent with pre-jet-break expectations, assuming $p \approx 2.2$, an ISM-type CBM and $\nu_m, \nu_a < 8.5$ GHz $< \nu_c$; a post-break slope with edge effect and $\nu_a < 8.5$ GHz $< \nu_m < \nu_c$ is within $\sim 1.7\sigma$.

Our fitting process is done ignoring the radio reverse shock (< 4 d). We also ignore the optical points before 0.05 d, as these seem to be the tail end of an achromatic flare visible all the way to the γ rays (Cenko et al.

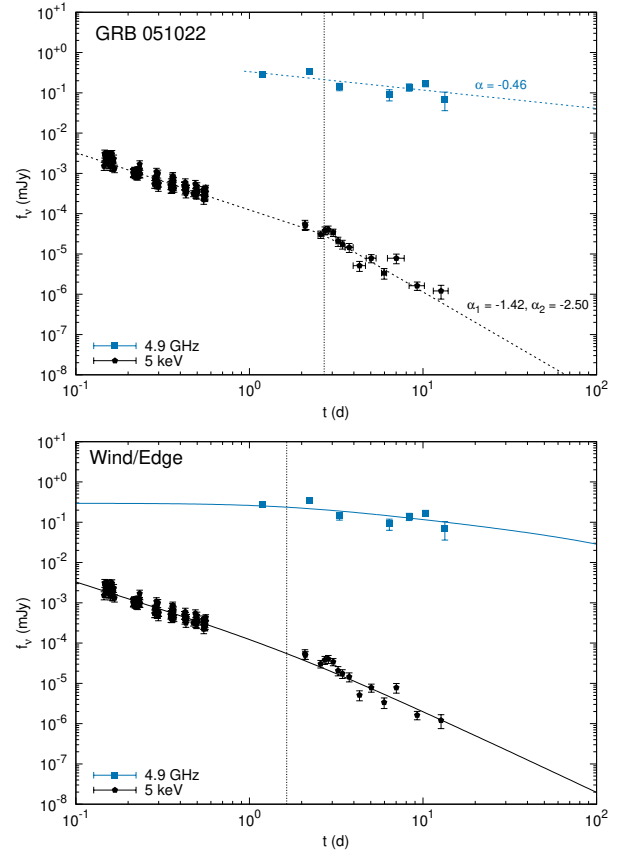


Figure 2. Our single and broken power law fits (upper panel) and best-fitting analytical model (lower panel) compared to the light curves of GRB 051022.

2006). Our best-fit model can account for all of the features of the light curve, but requires a very low ISM density ($\sim 10^{-5}$ cm $^{-3}$) and a very small opening angle (0.024 rad, or ~ 1.4 deg). If one restricts these parameters to more typical values (e.g. $\theta_j > 0.05$ rad and $n_0 > 10^{-4}$ cm $^{-3}$), the radio points are consistently over-predicted, while with wind CBM, they are under-predicted. We thus consider GRB 050820A tentatively consistent with standard theory. Cenko et al. (2006) argued that the radio emission of this burst was particularly weak and incompatible with the standard model, although they did not attempt a full multi-wavelength model fit. Cenko et al. (2010), on the other hand, did, and consistently under-predicted the radio data instead. Their model (from Yost et al. 2003) used break frequencies and fluxes from Sari et al. (1998) and Granot et al. (1999a,b) instead of the more recent Granot & Sari (2002), which may explain the discrepancy.

3.2. GRB 051022

A possible jet break was observed in the X-ray (with $P_F = 0.82$, the break is ambiguous); however, as this

was a dark burst, an optical afterglow was not detected (Fig. 2). The X-ray light curve is consistent with $p \approx 2.5$ and $\nu_c, \nu_m < \nu$. The radio light curve has a large scatter, but Rol et al. (2007) attribute this to scintillation effects; a single power law with strong scintillation may thus fit the light curve. In this case α_{radio} is consistent with the $-1/3$ expected for a post-jet-break slope if $\nu < \nu_m$ and with full lateral expansion. Alternatively one can place a rise before ~ 2 d, but then $\alpha_{\text{radio}} = -0.67 \pm 0.28$. This is still consistent with $-1/3$ within $\sim 1.2\sigma$, however, if ν_m stays above 4.9 GHz until ~ 15 d. With an edge effect jet break (1.1σ consistent with observations in the ISM scenario), the radio decline is also consistent with post-jet-break if $\nu_a < 4.9 \text{ GHz} < \nu_c < \nu_m$. Our model fit adequately reproduces the light curve, though the best-fit $\theta_j = 0.03 \pm 0.01$ is somewhat low; the best fit has a wind-type CBM, but an ISM-type CBM produces a fit of comparable quality. Therefore GRB 051022 is consistent with the standard model. Rol et al. (2007) also achieve a good fit; their model does not include IC effects and assumes lateral expansion, but their parameters other than p are consistent with ours.

3.3. GRB 070125

Chandra et al. (2008) place an optical break $\gtrsim 3\times$ earlier than the X-ray break, the latter delayed by effects from IC emission and not visible in the light curve. This is supported by the r -band light curve, which seems to steepen at ~ 3 d, although the data are sparse here. However, if this is a jet break, the preceding slopes in r (-1.66 ± 0.10) and X-ray (-2.00 ± 0.09) match an ISM-type CBM and $\nu_m, \nu_a < r < \nu_c < 5 \text{ keV}$, but this requires $p \sim 3.2$. If the jet break is in fact earlier and we have measured the post-jet-break slopes, this implies $p \sim 2.3$ and no lateral expansion. The apparent plateau in the optical at < 1 d may be due to ν_m passage in either case.

The radio light curve (Fig. 3) shows consistency with a single power law at all fitted frequencies after a peak between 10 and ~ 30 d, but at 8.5 GHz we see an ambiguous ($P_F = 0.852$) break at 88 ± 41 d as well. The other frequency with an equally long follow-up, 4.9 GHz, does not share this feature, however, and the putative post-break slope is only -1.12 ± 0.32 . The radio slopes are inconsistent with scenarios allowed by the optical and X-ray bands. The spectral index below 22.5 GHz evolves from 1.23 ± 0.11 at 15 d to 0.47 ± 0.04 at 87 d, indicating that ν_a is located slightly above 22.5 GHz, but the slope of the light curve at 14.9 and 22.5 GHz before this time ($\alpha \approx -0.55$) does not match the $\alpha \geq -1/4$ predicted below ν_a after the jet break.

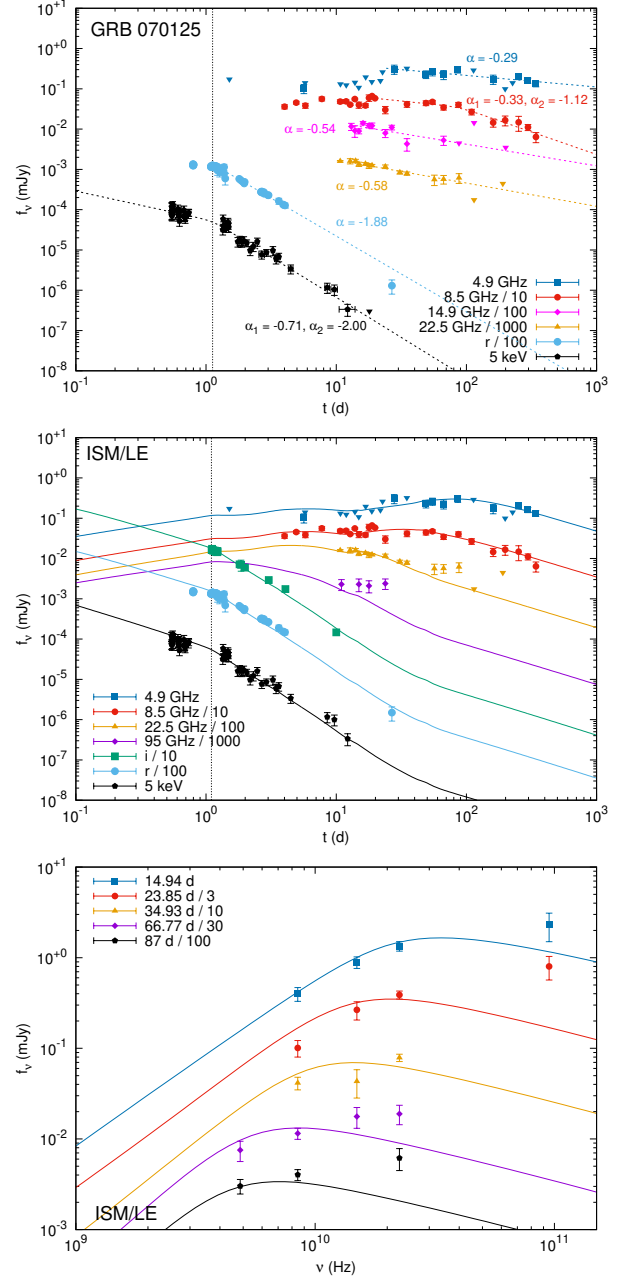


Figure 3. Our single and broken power law fits (upper panel) to the light curves of GRB 070125, and our best-fitting analytical model compared to the light curves (middle panel) and radio SEDs (lower panel). Two additional optical frequencies used in the fitting are omitted from this figure for clarity.

Chandra et al. (2008) note a lack of good radio fits to their model, but mostly bring up the early times, where they interpret the difference as scintillation effects. Their model, based on Yost et al. (2003), underpredicts the radio data points at > 200 d and, in the case of 8.46 GHz, also at < 10 d. Our fitting code can roughly reproduce the X-ray, optical, 4.9 GHz and 8.5

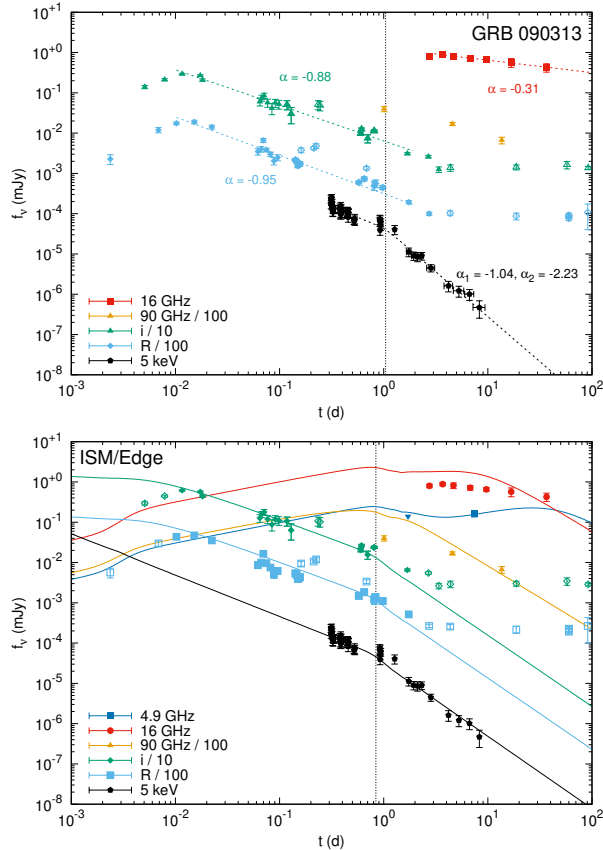


Figure 4. Our single and broken power law fits (upper panel) and best-fitting analytical model (lower panel) compared to the light curves of GRB 090313. Four additional frequencies with one data point each, used in the fitting, are omitted from this figure for clarity.

GHz light curves (with a jet break much earlier than suggested by Chandra et al. 2008), but under-predicts the late-time fluxes at 22.5 and 95 GHz. The shape of the SED clearly deviates from the model after 15 d. Therefore we consider GRB 070125 problematic for the standard model.

3.4. GRB 090313

The X-ray behavior is consistent with $p \approx 2.2$ and $\nu_c < \nu$. The initial ($\lesssim 0.01$ d) rise of the optical light curve can be explained by a decelerating fireball when ν_m lies below the optical bands (Melandri et al. 2010). The light curve also exhibits a rebrightening feature starting at ~ 0.2 d. This ‘bump’ in the light curve may be due to a density variation in the CBM. Delayed energy injection is another option, but the post-injection optical light curve would then become much steeper than the X-ray decline. The radio light curve (Fig. 4) peaks around $3 \times t_{j,X}$ and turns over onto a single power law with $\alpha_{16\text{GHz}} = -0.31 \pm 0.01$. This is close to $-1/3$ expected after a lateral expansion break when

$\nu < \nu_m$, so GRB 090313 at first glance seems compatible with the standard model, if ν_m stays above 16 GHz until ~ 35 d. The optical spectral index of this GRB, staying approximately constant around -1.1 (Melandri et al. 2010), indicates either that $\nu_m, \nu_c < i$ or that the optical data are affected by extinction.

Melandri et al. (2010) argue that the rise to the ~ 0.01 d deceleration peak requires ν_m to be below optical at the start of the light curve. Our code does not include the deceleration peak, but we can address this by ignoring the points before 0.01 d while introducing an additional constraint: unless $\nu_m < R$ at ~ 0.003 d, a zero likelihood for the model is returned. The optical bump at 0.2–0.5 d was ignored in our model fits as well – as were the points affected by the host galaxy after 2 d. In the fit, ν_m cannot stay above 16 GHz long enough to reproduce the observed shape of the light curve, and the model attempts to fit it with a smooth transition to regime 2. The radio points above 5 GHz are over-predicted until late times, where a steepening to a t^{-p} decline is predicted, but not seen in the data. We do not consider GRB 090313 consistent with the standard model.

3.5. GRB 110709B

GRB 110709B was a dark burst that was not detected in the optical. The X-ray behavior (Fig. 5) is consistent with $p \approx 1.9$ and $\nu_c, \nu_m < \nu$ or with $p \approx 2.2$ and $\nu_m, \nu_a < \nu < \nu_c$ in ISM using standard closure relations. Thus we use Eqs. (4)–(7) of Dai & Cheng (2001) for $1 < p < 2$. Here, we find an X-ray post-jet-break slope consistent with $p \approx 1.8$ and $\nu_c < \nu$ and an edge effect in ISM (albeit only at 1.8σ), while in wind the observed $\Delta\alpha = 0.66 \pm 0.05$ is between lateral expansion and edge effect. The radio light curve at 5.8 GHz declines consistently with a pre-jet-break light curve when $p \approx 1.8$, $\nu_m < 5.8$ GHz and in an ISM-type CBM, but if the slope is indeed pre-break in the radio, places a limit of $t_{j,\text{radio}} \gtrsim 60t_{j,X}$ assuming that $t_{j,\text{radio}}$ is after the last radio detection. These results do not change when using standard closure relations, except that $p \approx 1.9$ instead. No post-jet-break scenario allowed by the X-ray light curve is consistent with the radio power law.

Both our fitting code and Zauderer et al. (2013) do, however, find a wind model that provides a reasonable fit to the radio if the post-jet-break light curve starts steepening around 50 d. The parameters of the fits are somewhat different, but Zauderer et al. (2013) did not include IC effects in their model. We find a roughly equally good fit with both types of CBM; our wind fit is shown as its χ^2 is slightly better. GRB 110709B thus remains consistent with the standard model.

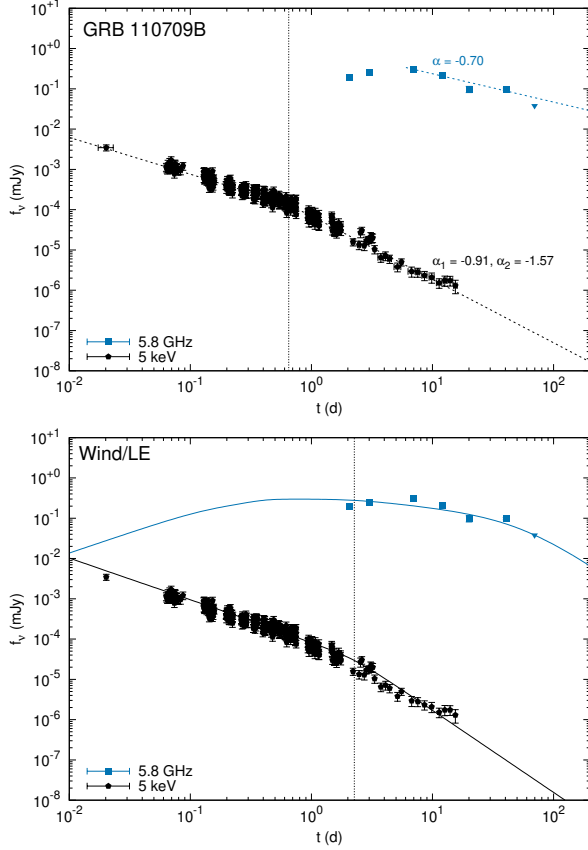


Figure 5. Our single and broken power law fits (upper panel) and best-fitting analytical model (lower panel) compared to the light curves of GRB 110709B.

3.6. GRB 120326A

GRB 120326A is the only event in this sample with an apparent jet break clearly observed below ~ 100 GHz; this happens at $\sim 44.7 \pm 15.3$ d at 19.2 GHz, roughly 30 times later than the observed (albeit ambiguous; $P_F = 0.82$) X-ray jet break. The jet break is clearer in the optical. At 93 GHz the steepening occurs around 10 d. The post-break decline at all radio frequencies is highly uncertain, but consistent with the X-ray and optical decline. The X-ray and optical light curves imply $p \approx 2.3$ and a lateral expansion break in an ISM-type CBM. Before the steepening at ~ 45 d, the slope of the radio decline is seemingly inconsistent with theoretical expectations in this scenario.

This burst had a re-brightening episode before ~ 0.5 d, for which Laskar et al. (2015) used a model with energy injection. As they point out, the behavior of the burst should be similar to the standard model without energy injection after this time. We therefore fit the light curves starting at 0.5 d. Our model reproduces the shapes of the radio (with a smooth transition from $t^{-1/3}$ to t^{-p}) and optical light curves, but the X-ray flux is under-

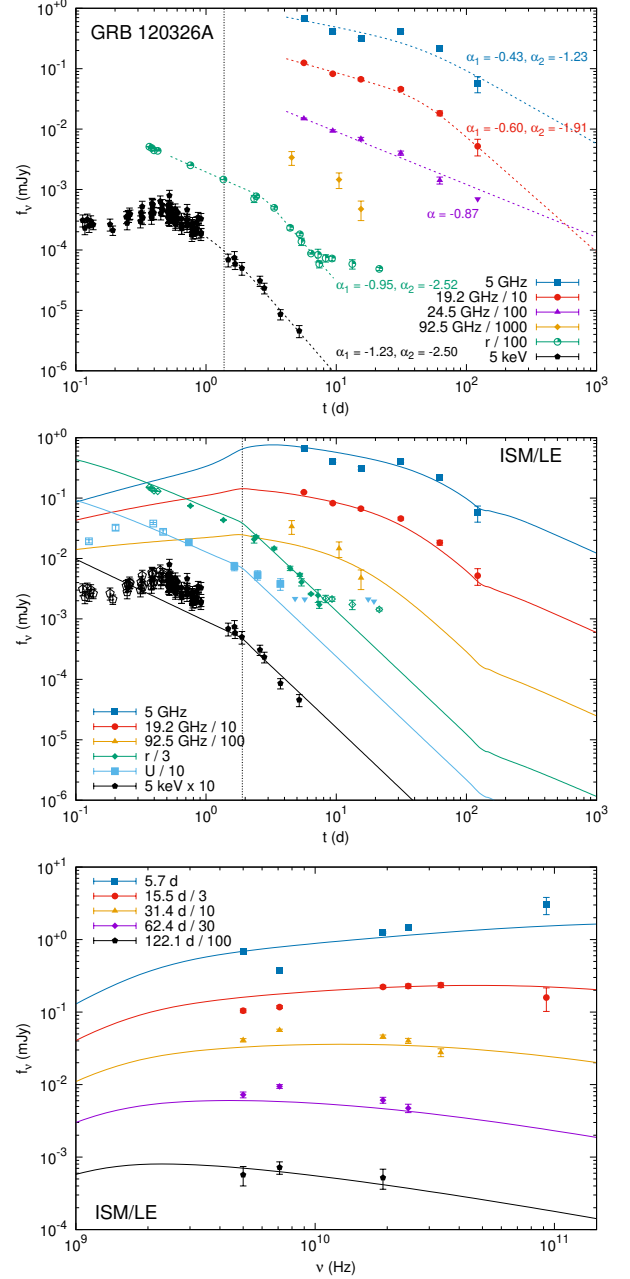


Figure 6. Our single and broken power law fits to the light curves of GRB 120326A (upper panel), and our best-fitting analytical model compared to the light curves (middle panel) and radio SEDs (lower panel). Ten additional optical and radio frequencies used in the fitting are omitted from the light curve figure for clarity.

predicted at $t < 1$ d by a factor of a few and the steepening in the millimeter light curve is slightly later than observed. Laskar et al. (2015) obtained a nearly identical fit (apart from the non-relativistic transition) with similar parameters, and also under-predicted the X-ray flux. Both our best fit and Laskar et al. (2015) also place ν_m and ν_c below both optical and X-ray, but the

power-law fit to the early X-ray is steeper than the optical by $t^{-0.28 \pm 0.20}$, implying that $\nu_m < r < \nu_c < 5$ keV. However, the optical and X-ray slopes are still within 1.4σ . Nonetheless, the standard model seems to have a problem reproducing the afterglow after the energy injection.

3.7. GRB 130907A

The X-ray light curve exhibits a jet break at ~ 0.2 d (Fig. 7). The pre-jet-break X-ray behavior is consistent with $p \approx 2.4$ and $\nu_c < \nu$ in ISM, or $p \approx 2.2$ and $\nu < \nu_c$ in wind. The X-ray spectrum has an index of $\beta_X = -0.69 \pm 0.06$ at 0.2 d (Veres et al. 2015), which implies $p = 2.38 \pm 0.12$ – after the jet break, on average, $\beta_X = -0.96 \pm 0.05$ implying a ν_c passage. In order to match the early X-ray-to-optical spectrum to a synchrotron model, one requires a host extinction of $A_V \approx 1.3$ mag and $\nu_m < i < 5$ keV $< \nu_c$ at 0.2 d (Veres et al. 2015). The post-jet-break slope is $\alpha_2 = -2.2 \pm 0.03$. Taken together, these observables seem to favor the wind scenario with lateral expansion and $p \approx 2.2$.

The radio decline is a single power law inconsistent with the above scenario. Veres et al. (2015) described the radio evolution with a $-3(p-1)/4$ decline, which would result in $p \approx 2.0$ and, furthermore, requires an ISM-type CBM. Since this refers to a pre-break slope, the radio break would also be delayed: $t_{j,\text{radio}} \gtrsim 170t_{j,X}$ – the longest relative delay in this sample. To account for this, Veres et al. (2015) attempted to explain the burst without a jet break and to describe the behavior at all frequencies as being pre-jet-break – in this scenario the break in the X-ray light curve would be a combination of a ν_c passage and a transition from wind-like CBM to ISM-like. They were unable to reconcile this scenario with the steepness of the X-ray decline, though, and also suggested a combination of a narrow jet responsible for the X-ray emission and a wide jet responsible for the lower frequencies. The radio decline does match an edge effect break with wind and $\nu_a < \nu_c < 15$ GHz $< \nu_m$, but this would not allow the 15 GHz light curve to rise after t_j as observed.

For fitting, we fix extinction at $A_V = 1.3$, as the X-ray-to-optical spectrum seems to require it. Our fitting code is unable to fit any of the wavelengths well. A t^{-p} decline is predicted in the radio, but not seen in the data. The deviation is driven by the radio data: a better fit to the optical and X-ray can be obtained by ignoring the early (< 10 d) radio points, but even then only with $p > 3$. Thus we consider this GRB inconsistent with the standard model.

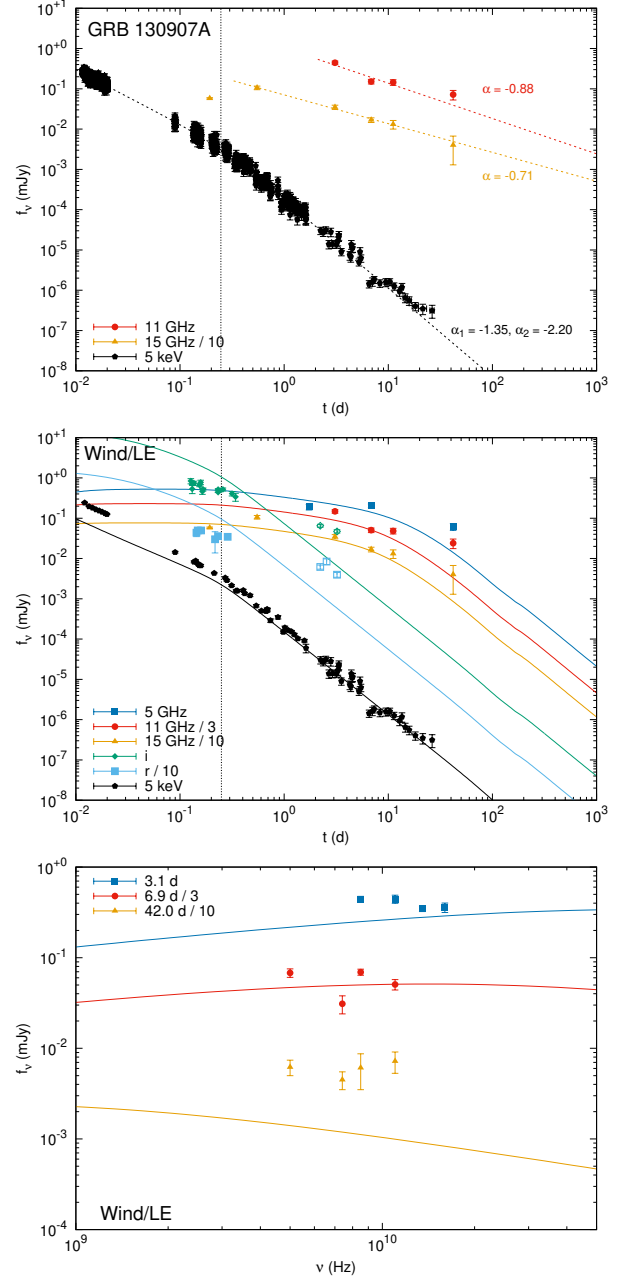


Figure 7. Our single and broken power law fits to the light curves of GRB 130907A (upper panel), and our best-fitting analytical model compared to the light curves (middle panel) and radio SEDs (lower panel). Twelve additional optical and radio frequencies used in the fitting are omitted from the light curve figure for clarity.

3.8. GRB 141121A

This ultra-long GRB shows peculiarities both in X-ray and in radio (Fig. 8). The X-ray decline after the early steep decline ($\gtrsim 0.4$ d) is a broken power law, and the decline after the last break at ~ 4 d matches expectations for a post-jet-break decline with $p \approx 2.2$ and

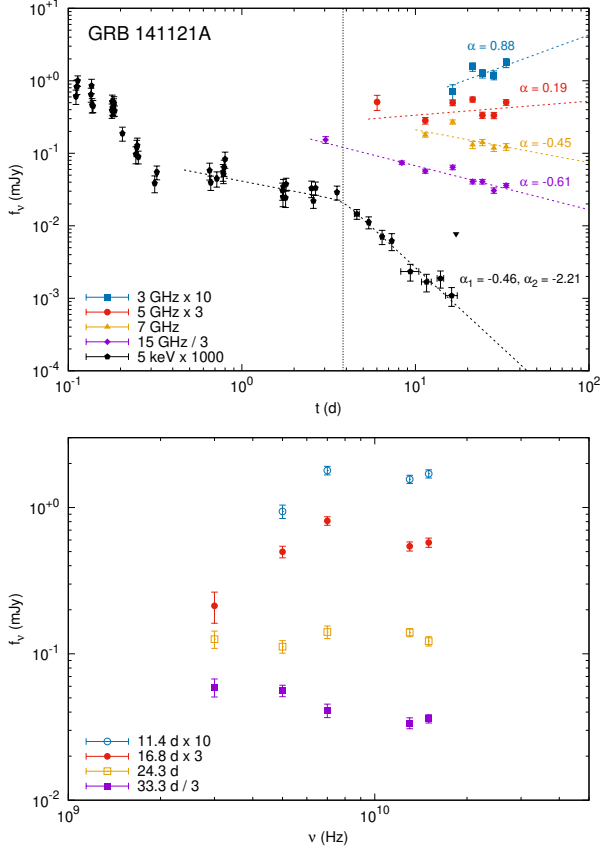


Figure 8. Our single and broken power law fits to the light curves of GRB 141121A (upper panel) and the radio SEDs of this burst (lower panel).

full lateral expansion, or $p \gtrsim 2.6$ without it. The slow decline before ~ 4 d – almost a plateau – may be the product of late engine activity. The radio light curve at 15 GHz fits a single power law, consistent with an edge effect jet break, ISM and $\nu_a < \nu < \nu_c < \nu_m$ or with a pre-break slope, wind and $\nu_a < \nu < \nu_c < \nu_m$. The frequencies below 15 GHz show a more complex light curve, but its slope flattens and even becomes positive with decreasing frequency – in this case, we also fit the rising light curves – which also fits the pre-jet-break slope if $3 \text{ GHz} \lesssim \nu_a \lesssim 15 \text{ GHz}$ until ~ 30 d. In this case we can place a limit of $t_{j,\text{radio}} > 8 \times t_{j,X}$ based on the last radio detection. The 3 GHz rise is too steep for the post-jet-break scenario. The complex optical and radio light curve was interpreted by Cucchiara et al. (2015) using a model with energy injection into a reverse shock and a two-component jet. However, even this model does not fit the early radio points very well. The possible influence of a reverse shock is also seen in the spectrum, which shows some evidence of multiple peaks until 33.3 d. The complexity of the light curve and spectrum means our fitting code is naturally unable

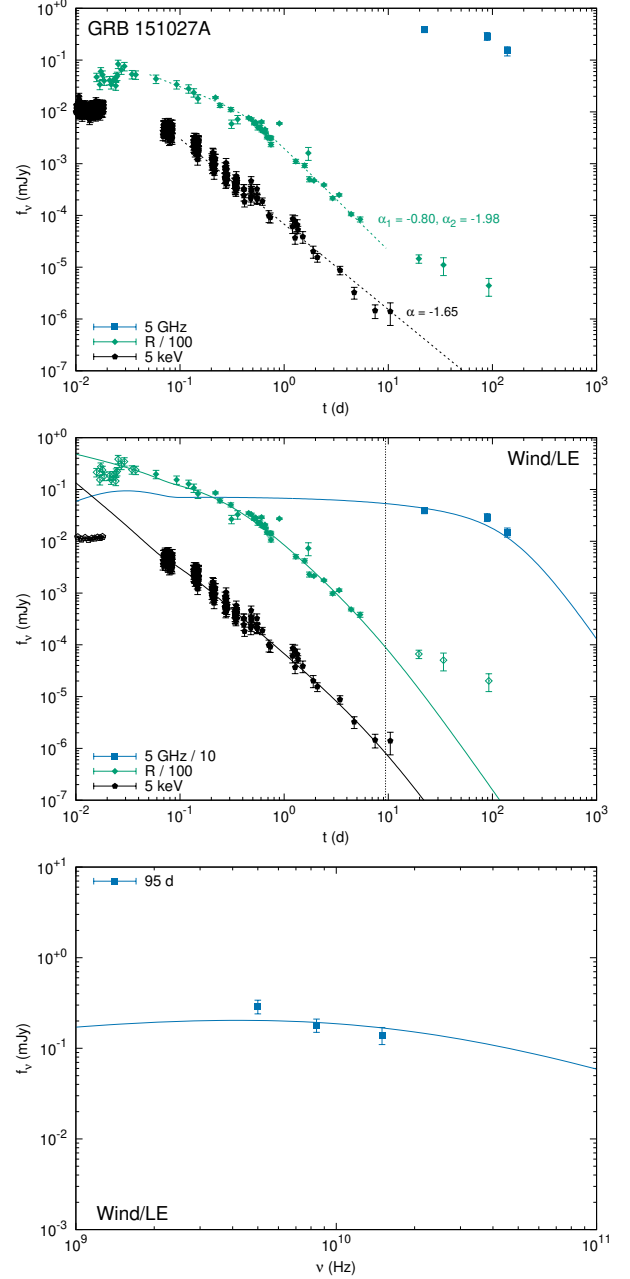


Figure 9. Our single and broken power law fits to the light curves of GRB 151027A (upper panel), and our best-fitting analytical model compared to the light curves (middle panel) and radio SEDs (lower panel). Three additional radio frequencies with one data point each used in the fitting are omitted from the light curve figure for clarity.

to reproduce the observations, and is therefore not used here. We consider GRB 141121A inconsistent with the standard model.

3.9. GRB 151027A

GRB 151027A exhibited a plateau in its early optical and X-ray light curve. The model favored by Nappo

et al. (2017) incorporated a phase of late prompt emission to accommodate this. We ignore the plateau phase of the light curve ($\lesssim 0.05$ d) in our fits; both the X-ray and optical light curves steepen after this. After 10 d, the optical light curve flattens, possibly because of supernova emission; this part is also ignored.

The X-ray light curve declines steeply enough to match our sample criteria; but only the optical light curve has a feature that looks like a jet break. After 0.5 d, the optical slope is steeper than the X-ray by $t^{-0.33 \pm 0.14}$, which is consistent with $\nu_m < R < \nu_c < 5$ keV in a wind-type CBM. The slope of the optical light curve before this is inconsistent with this scenario, however.

Our best model fit to the post-plateau light curves reproduces the X-ray, optical and radio data. With a wind model, the steep decay is reproduced with no jet break until the end of the observed light curve. It does require a high p , however: $p = 2.91^{+0.07}_{-0.09}$. Thus we consider GRB 151027A tentatively consistent with the standard model. The shape of the X-ray-to-optical spectrum, which Nappo et al. (2017) considered a sign of the late prompt component, is addressed in our model by host galaxy extinction. Their late prompt emission model is, of course, also plausible as this extra component and the early plateau are not included in our code.

3.10. GRB 160509A

This burst was well observed in the X-ray, but an optical break was not observed due to a high extinction (although K20 did see a late-time slope consistent with post-jet-break expectations; see Fig.10). The radio light curves at 6 and 9 GHz (with the longest follow-up) are consistent with a pre-jet-break slope assuming $6 \text{ GHz} > \nu_m$ in an ISM-type CBM and $p \approx 2.2$, which is also consistent with the X-ray. The break time in X-rays is ~ 3.5 d (K20), resulting in a limit of $t_{j,\text{radio}} > 20 \times t_{j,X}$ based on the last radio detection if the slope is indeed pre-break. Alternatively, the radio slope is consistent with ISM, edge effect and $\nu_a < \nu_c < \nu < \nu_m$, which the sparse optical data do not rule out, but this would place ν_c below 6 GHz at 10 d, which does not fit the radio-to-optical spectrum with $\beta = -0.40 \pm 0.01$ (K20). A reverse shock was detected in this GRB (Laskar et al. 2016). The spectrum initially shows a moving peak associated with the reverse shock, but after its passing ($\gtrsim 10$ d based on the light curves) the spectrum becomes almost flat. This could in principle be due to a combination of reverse shock contribution and a smooth ν_m or ν_c break around the observed frequencies.

Our best-fit model with an ISM-like CBM does reproduce a flat radio SED at late times, and fits the light

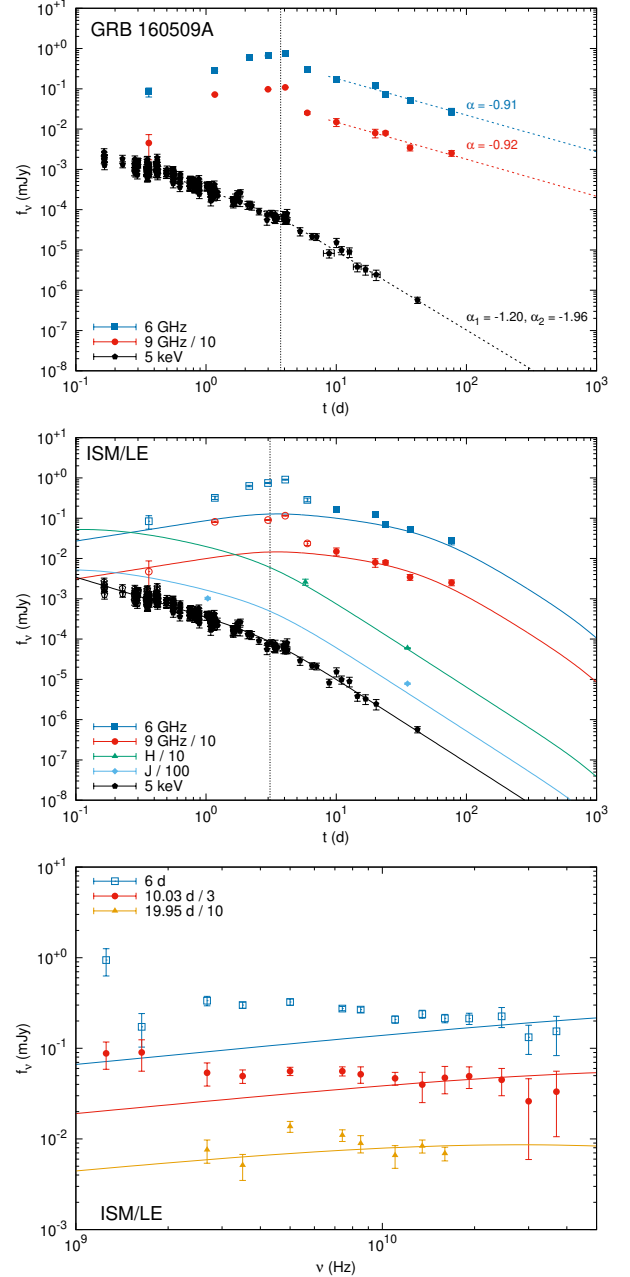


Figure 10. Our single and broken power law fits to the light curves of GRB 160509A (upper panel), and our best-fitting analytical model compared to the light curves (middle panel) and radio SEDs (lower panel). Five additional optical and radio frequencies used in the fitting are omitted from the light curve figure for clarity.

curves at all frequencies reasonably well. This requires a smooth ν_m passage through the radio bands between 10 and 100 days in order to be consistent with the observed decline. Thus, provided that the $\sim t^{-2}$ decline in the radio starts around the last observed epoch, and the flat spectral shape around 10 d can be attributed to lingering contribution from the reverse shock, GRB

160509A is consistent with the standard model. The parameters of our best fit differ somewhat from Laskar et al. (2016), but using their parameters also results in a reasonable fit by eye, and they lacked access to the late-time data in K20.

We note that K20 used the numerical fitting code BOXFIT (van Eerten et al. 2012), and their best fit was only consistent with the late-time points ($\gtrsim 30$ d), underpredicting the radio fluxes until then. Furthermore, even this required a jet break ~ 10 times later than the broken power law fit indicates. This suggests that either the analytical or numerical model (or both) is erroneous. A further difference between the models was the extremely late jet break in the best-fit wind model – and in a BOXFIT light curve produced using the best wind parameters of Laskar et al. (2016) (neither of which fit the radio light curve). An ISM model with their parameters produced a similar result as the best fit.

3.11. GRB 160625B

An optical and X-ray jet break was seen at ~ 20 d (K20). The radio light curve (Fig. 11) at 6.1 GHz is again consistent with a pre-break slope assuming $\nu_m < \nu$ in an ISM-type CBM, with a slope corresponding to $p \approx 2.4$, which is close to the value of $p \approx 2.3$ determined through the early X-ray and optical light curve. Thus a limit of $t_{j,\text{radio}} > 10 \times t_{j,\text{optical}}$ can be placed if the pre-break scenario holds. No post-break slope allowed by the higher frequencies – which imply ISM, $p \approx 2.3$ and $\nu_m, \nu_a < \nu_c$ – is consistent with the radio. This burst also showed signs of a reverse shock (Alexander et al. 2017), at low frequencies ($\lesssim 5$ GHz) until ~ 20 d. After this, similarly to GRBs 130907A and 160509A, the radio SED becomes flat.

In our fitting, we ignore radio points at < 20 d because of the reverse shock. Since Alexander et al. (2017) point out a possible extreme scattering event affecting the lowest radio frequencies, we also ignore all < 5 GHz data. Our best-fit model is able to reproduce the observed behavior at optical and X-ray frequencies. However, the shapes of the 6.1 GHz light curve and the SED deviate somewhat from the model, the former both at early times (~ 20 d) and at the last radio point (~ 200 d). Furthermore, the model once again predicts a $\sim t^{-2}$ decline starting soon after the last observed radio epoch. Therefore, considering the problems K20 had with fitting the light curve using BOXFIT as well, we consider GRB 160625B inconsistent with the model. Alexander et al. (2017) and Troja et al. (2017) found best-fit parameters similar to ours, but did not have the 210 d data point and placed a steepening at ~ 50 d.

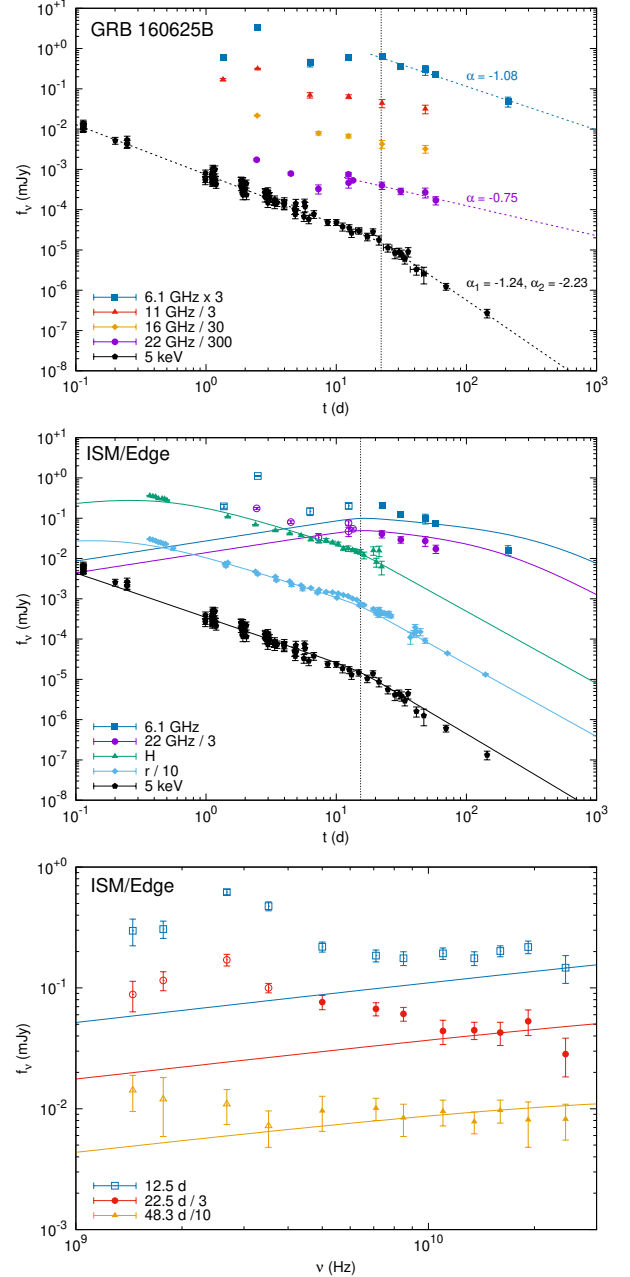


Figure 11. Our single and broken power law fits to the light curves of GRB 160625B (upper panel), and our best-fitting analytical model compared to the light curves (middle panel) and radio SEDs (lower panel). Eleven additional optical and radio frequencies used in the fitting are omitted from the light curve figure for clarity.

3.12. GRB 171010A

An X-ray break was seen for this burst, but the radio behavior (Fig. 12) was described as unusual by Bright et al. (2019). They attempted to explain the light curve evolution using a steep CBM density profile, but nonetheless found that the evolution of break frequen-

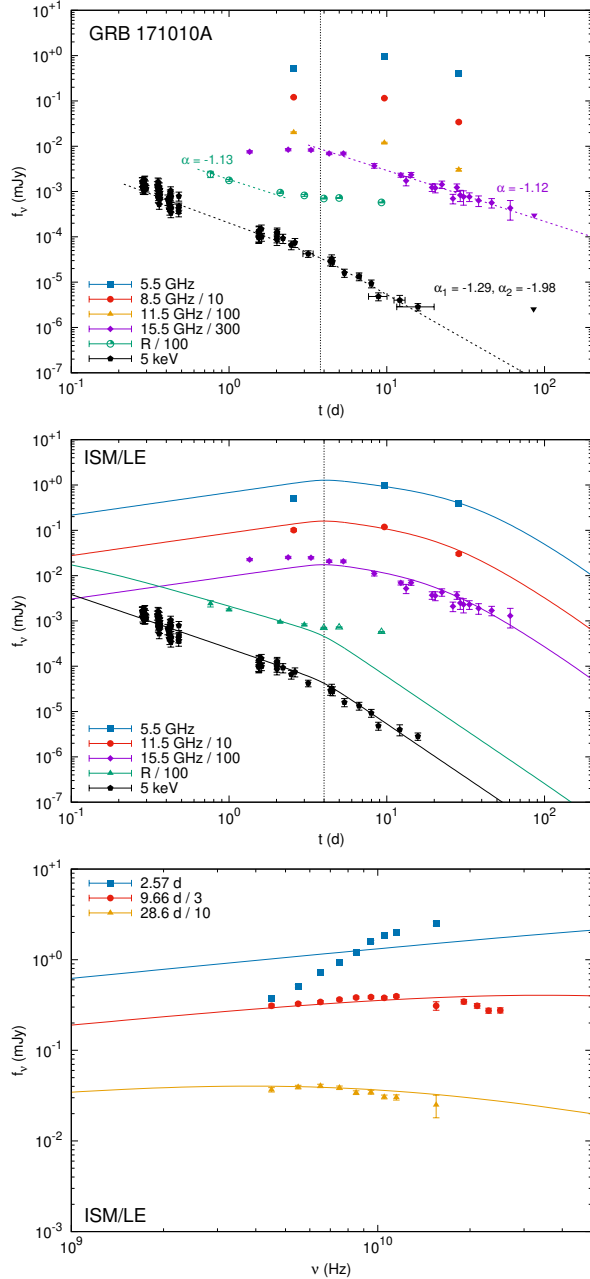


Figure 12. Our single and broken power law fits to the light curves of GRB 171010A (upper panel), and our best-fitting analytical model compared to the light curves (middle panel) and radio SEDs (lower panel). Ten additional optical and radio frequencies used in the fitting are omitted from the light curve figure for clarity.

cies in the spectrum seems too slow for the standard model to explain. The X-ray light curve is consistent with $p \approx 2.4$ with an edge-effect break, while the optical decline and the spectral index of $\beta = -0.87$ between optical and X-ray together imply that $R < \nu_c < 5$ keV in ISM. The radio decline slope of $\alpha = -1.12 \pm 0.05$ is consistent with $p \approx 2.5$ and pre-break. However, the

peak of the radio light curve is roughly simultaneous with the X-ray break, and thus GRB 171010A seems to exhibit another delayed radio break; we can place a limit of $t_{j,\text{radio}} > 13 \times t_{j,\text{X}}$ in this case based on the last radio detection. This requires that $\nu_m < 15.5$ GHz at $t_{j,\text{X}}$, while the first SED suggests 15.5 GHz $< \nu_m$ and $\nu_a \sim 10$ GHz. As Bright et al. (2019) point out, if the peak frequency is ν_m , its evolution is also slower than expected. No post-jet-break scenario allowed by the X-ray and optical is consistent with the radio decline.

Our own best-fit model agrees with the findings of Bright et al. (2019): individual SEDs can be reproduced by it, but not all epochs simultaneously. Specifically, our best-fit model disagrees with the earliest SED (~ 2.5 d). As for the light curve, instead of a single power law, our best fit is a smooth transition from $\nu_a < 15.5$ GHz $< \nu_m$ to $\nu_m < \nu_a < 15.5$ GHz. This prediction, however, deviates from the observed pre- t_j 15.5 GHz light curve. At other frequencies the light curve is sparse and such comparisons are more difficult. We consider GRB 171010A inconsistent with the standard model.

3.13. GRB 990510

For GRB 990510, only the optical shows evidence of a jet break (Fig. 13), but as the X-ray follow-up was much shorter, a break cannot be excluded in the X-ray. Both the optical and X-ray pre-break light curves are consistent with $p \approx 2.4$ and $\nu_m < \nu_c$ in an ISM-type CBM, but in this case the optical post-break decline may require a jet break mechanism that involves a combination of the edge effect and logarithmic lateral expansion, as seen in simulations by van Eerten & MacFadyen (2012). However, the post-optical-break radio decline can be fitted with $\alpha_{\text{radio}} = -0.62 \pm 0.10$, which is not compatible with any pre- or post-break slopes allowed by the higher frequencies. Our best-fit analytical model is able to reproduce the radio and optical light curves with a smooth transition from $\nu_a < 8.6$ GHz $< \nu_m$ to $\nu_m < \nu_a < 8.6$ GHz, but in this case a t^{-p} decline is predicted soon after the last radio observations. We conclude that GRB 990510 is consistent with the standard model if a t^{-p} decline began soon after the radio observations ended. A similar quality fit was obtained by Panaitescu & Kumar (2001), but as they use different equations for break frequencies and flux, they arrive at different parameters.

3.14. GRB 991208

No X-rays were detected for this GRB, but we can use the optical light curve (Fig. 14) to infer that $p \approx 2.4$ – assuming lateral expansion – and that the jet break happened some time before the optical observations ($\lesssim 2$ d).

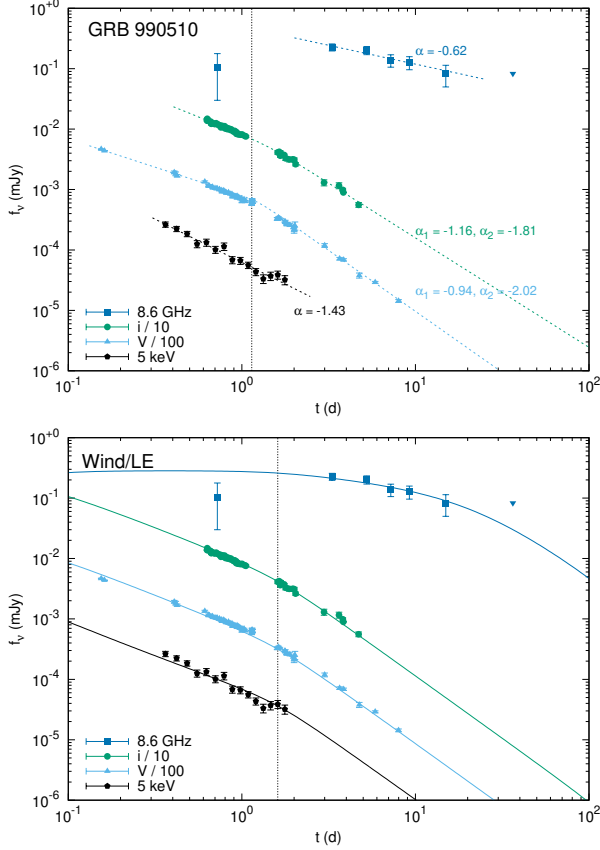


Figure 13. Our single and broken power law fits (upper panel) and best-fitting analytical model (lower panel) compared to the light curves of GRB 990510. Four additional optical and radio frequencies used in the fitting are omitted from the light curve figure for clarity.

Without lateral expansion, assuming $p < 3$, the optical slope implies $\nu_a, \nu_c, \nu_m < \nu$ in ISM or $\nu_a, \nu_m < \nu < \nu_c$ in wind. The 8.5 GHz light curve is consistent with post-jet-break in the $\nu_a < \nu_c, 8.5 \text{ GHz} < \nu_m$ scenario, but also with a pre-jet-break slope with $p = 2.4, \nu_a, \nu_m < 8.5 \text{ GHz} < \nu_c$ in ISM. The spectrum, however, implies that $\max(\nu_m, \nu_a) > 10 \text{ GHz}$ until at least $\sim 50 \text{ d}$. The slope continues until $\geq 300 \text{ d}$, i.e. in the pre-jet-break case we can set a limit of $t_{j,\text{radio}} \gtrsim 140t_{j,R}$ using the last radio detection. In a wind-type CBM, the radio slope is consistent with post-jet-break expectations, t^{-1} , if the fast-cooling spectrum (i.e. $\nu_m > \nu_c$) persists until late times.

Our best-fit model (with wind-type CBM and lateral expansion) can reproduce the shapes of the SEDs and the light curves reasonably well – albeit with some deviation at 1.43 GHz – with a smooth transition from $\nu_a < 8.6 \text{ GHz} < \nu_m$ to $\nu_m < \nu_a < 8.6 \text{ GHz}$, followed by the onset of the non-relativistic phase at $\sim 50 \text{ d}$. It does slightly over-predict the optical points at $\sim 7 \text{ d}$,

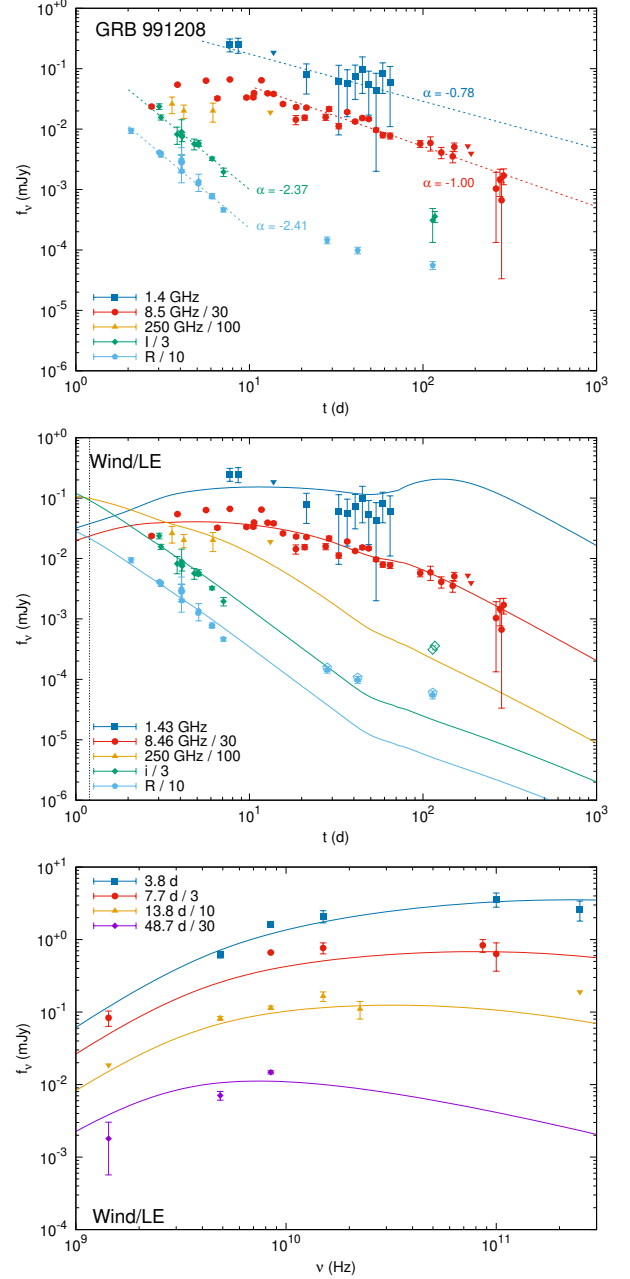


Figure 14. Our single and broken power law fits (upper panel) to the light curves of GRB 991208, and our best-fitting analytical model compared to the light curves (middle panel) and radio SEDs (lower panel). Nine additional optical and radio frequencies used in the fitting are omitted from the light curve figure for clarity.

though. Thus we conclude that GRB 991208 is tentatively consistent with the standard model. The preferred $\epsilon_e = 0.83^{+0.08}_{-0.10}$ is rather high, but setting an upper limit of $\epsilon_e < 0.7$ results in a fit of only slightly worse quality. It is worth noting, however, that this burst has no pre-jet-break data in any band, nor any X-ray data.

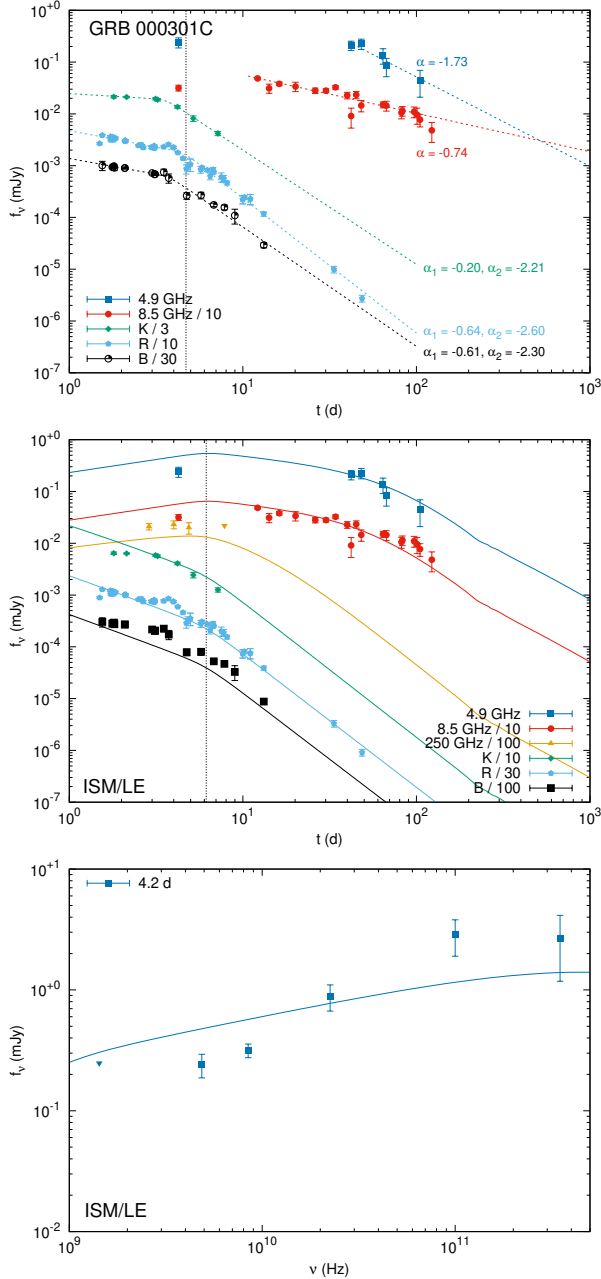


Figure 15. Our single and broken power law fits (upper panel) to the light curves of GRB 000301C, and our best-fitting analytical model compared to the light curves (middle panel) and radio SEDs (lower panel). Ten additional optical and radio frequencies used in the fitting are omitted from the light curve figure for clarity.

3.15. GRB 000301C

GRB 000301C was also not detected in X-rays, but a jet break was observed in the optical bands; the optical slope of $\sim t^{-2.6}$ (in the R band, with by far the longest follow-up among the optical bands) is too steep for an edge effect break, and thus implies $p \approx 2.6$. The K -

and B -band post-break slopes are not as steep, but the follow-up is shorter, which may affect the result. Berger et al. (2000) note fluctuations in the optical light curves that can explain the different fits to the different frequencies; these may be due to density changes in the CBM. Indeed, they (and our best-fit model below) suggest that the jet break occurred around the last K -band observation, and the “break” in K is merely the peak of a bump in the light curve. The perturbed optical light curve may also explain the large difference between pre- and post-jet-break slopes: in B and R , the pre-jet-break slope is ~ -0.6 , seemingly incompatible with $p = 2.6$, and the K -band decline is even shallower.

The radio decay seems much steeper at 4.9 than 8.6 GHz, but this is plausibly due to the smaller number of data points, none of them between 10 and 40 d, with much larger errors. The better-sampled 8.6 GHz decay can be fitted with a single power law from ~ 10 to $\gtrsim 100$ d. This power law ($t^{-0.74 \pm 0.07}$) is not consistent with post-jet-break expectations with lateral expansion, but within 1.1σ of the pre-break $t^{-2/3}$ in a wind CBM and $8.6 \text{ GHz} < \nu_c < \nu_m$ until $\gtrsim 20t_{j,R}$.

Our best-fit model does a good job of reproducing most of the radio and optical light curve (allowing for some optical deviation because of the aforementioned fluctuation) with a smooth post-jet-break ν_m passage. However, it has difficulty with the pre- t_j 250-GHz data, which it consistently under-predicts, while at 4.2 d, it places ν_a at a much lower value than the observations indicate. Berger et al. (2000) were able to better reproduce the radio SED, but the break frequencies in their model were free parameters instead of being determined by physical parameters. Thus, despite the lack of X-ray data to constrain the GRB, we consider GRB 000301C problematic for the standard model. Panaitescu (2005) used a structured jet model to describe GRB 000301C, but their fit is of similar quality as ours in the optical and worse in the radio.

3.16. GRB 000926

In the case of GRB 000926, the jet break seems to have been captured in the optical light curve, which is consistent with an edge effect jet break in ISM- or wind-type CBM at $\sim 1.4\sigma$ and $\sim 1.8\sigma$ respectively ($\Delta\alpha = -0.64 \pm 0.08$). The ISM scenario is disfavored by the pre-break optical decay. The best-sampled band, R , is consistent with $p \approx 2.5$ ($\nu_m < R < \nu_c$) or $p \approx 2.8$ ($\nu_c < \nu_m < R$) in wind, but requires $p > 3$ in ISM. The radio light curve decline is consistent with being post-jet-break in wind with edge effect and $\nu_a < \nu < \nu_m < \nu_c$. The decline is also close to the expected pre-jet-break slope in a wind CBM in the fast-cooling scenario, which

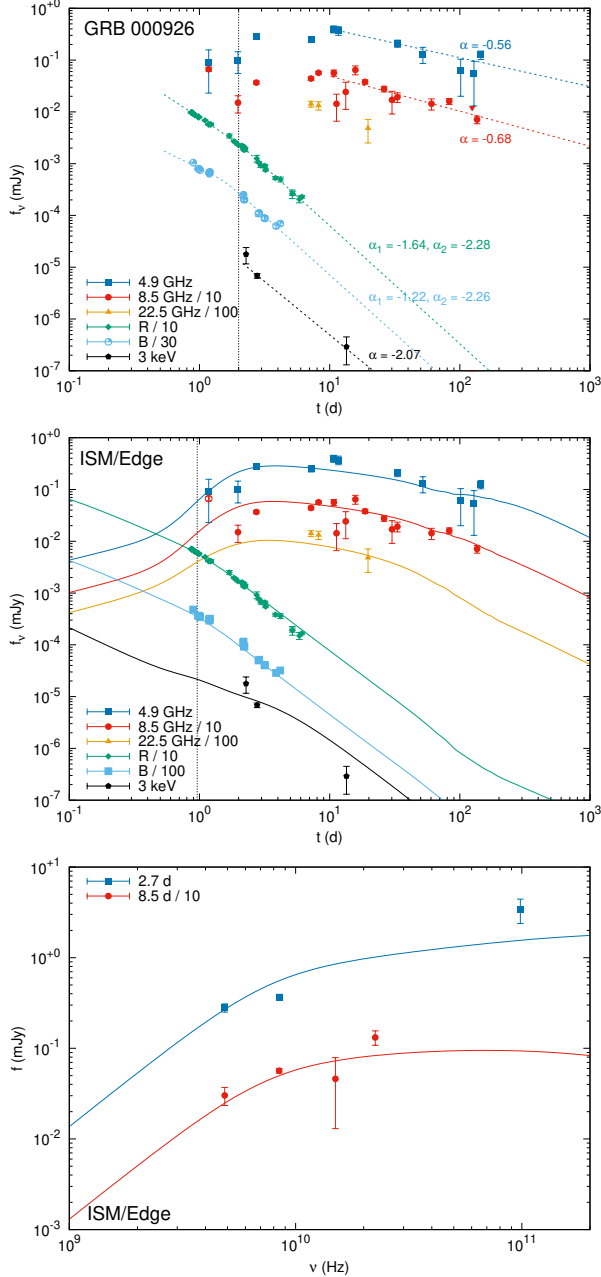


Figure 16. Our single and broken power law fits (upper panel) to the light curves of GRB 000926, and our best-fitting analytical model compared to the light curves (middle panel) and radio SEDs (lower panel). Seven additional frequencies used in the fitting are omitted from the light curve figure for clarity.

is plausible based on the optical and X-ray data. The radio light curve is rising or flat (the apparent scintillation at this time makes it difficult to tell) until $\sim 5t_{j,R}$, which is consistent with the above if the slope during the rise is $t^{1/2}$ and thus $\nu < \nu_a$.

Our best-fit model generally reproduces the shape of the optical and radio light curves. Harrison et al.

(2001) and Panaitescu & Kumar (2002) argued that the X-ray requires a contribution from IC emission, while Panaitescu (2005) was unable to explain the late-time radio behavior with a structured jet model. Our best fit in terms of χ^2 does not require IC emission, but instead imposes $\epsilon_B \approx 1$ – this requirement for models without IC effects was also noted by Harrison et al. (2001). By requiring a more typical value, $\epsilon_B < 0.1$, our model also needs IC emission; in this light we show this fit in Figure 16 and in Table 5. The shape of the radio and optical light curves is reproduced well, but there is a $\sim 3.5\sigma$ deviation at the last X-ray epoch. The X-ray light curve is sparse. Overall, we find GRB 000926 tentatively consistent with the standard model.

3.17. GRB 100418A

Based on the X-ray light curve (Fig. 17), we infer $p \approx 2.0$ and $\nu_c < \nu$, or alternatively $p \approx 2.3$ and $\nu_m < \nu < \nu_c$; in the latter case the CBM is restricted to ISM-like. The value of $\beta = -1.00 \pm 0.05$, reported by de Ugarte Postigo et al. (2018) to fit the spectrum from optical to X-ray at ~ 2 d, rules out the former unless ν_c is also below the optical bands. The radio light curve at 5 and 8.5 GHz peaks around 50 d ($10 \times t_{j,X}$) and at each frequency settles onto a power law decay, though the power-law index varies substantially with frequency. At 90 GHz, the maximum of the light curve takes place at $t \lesssim 1$ d, and the slope thereafter is consistent with pre-jet-break and $p \approx 1.8$, meaning $t_{j,90 \text{ GHz}} \gtrsim 15t_{j,X}$ if the slope is indeed pre-break. With such a low p we also need to use Eqs. (4)–(7) in Dai & Cheng (2001) for $p < 2$. We find that the 90 GHz and X-ray light curves are both consistent with $p \approx 1.5$ and an ISM-type CBM, with $\nu_c < 5$ keV, and $\nu_m < 90 \text{ GHz} < \nu_c$, but the other radio frequencies are not. No other $p < 2$ scenario is consistent with both X-ray and millimeter frequencies.

Moin et al. (2013) suggested that the late peak epoch seems to require a model of late energy injection that revitalizes the forward shock. With a re-energized shock one would still expect the evolution beyond the late-time peak to resemble the post-peak evolution of the ‘standard’ case; but a post-jet-break decline is not seen at any point in the radio. It is, however, possible that there is a second peak in the 90 GHz light curve around 25 d, in which case the slope before its onset could in principle be steeper; but this is not seen convincingly in the data. The peaks in the radio light curves seem to roughly correspond to ν_m passage based on the SED evolution; thus the late injection model remains plausible.

Laskar et al. (2015) attempted to model this burst using an energy injection episode at $\lesssim 0.5$ d; they considered strong scintillation a possible explanation for the

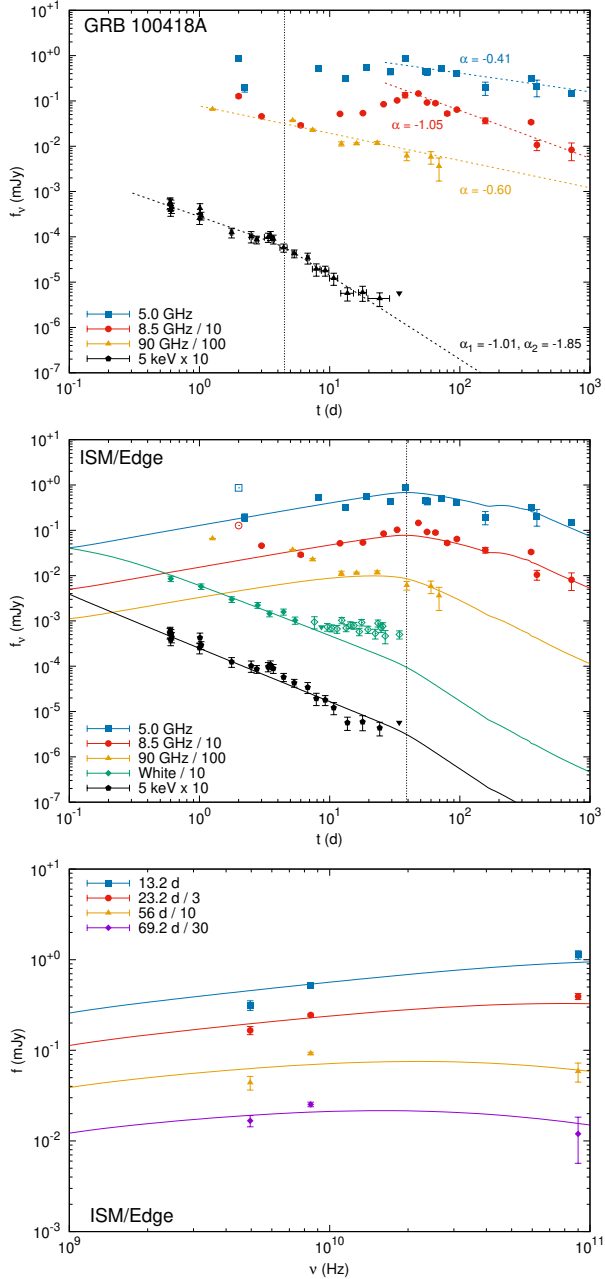


Figure 17. Our single and broken power law fits (upper panel) to the light curves of GRB 100418A, and our best-fitting analytical model compared to the light curves (middle panel) and radio SEDs (lower panel). Eight additional optical and radio frequencies used in the fitting are omitted from the light curve figure for clarity.

shape of the radio light curve between 2 and 20 days, and ignored these data points in their fitting process. By doing this, they were able to fit the light curve. They did not, however, have access to 4.8 GHz data in the same time period from [de Ugarte Postigo et al. \(2018\)](#), which behave roughly the same way as the 8.5 GHz data. We attempt a fit as well (ignoring the very bright first points

of the 5.0 and 8.5 GHz light curves instead, along with the pre-injection points at < 0.5 d), and find that most of the features of this GRB can be roughly reproduced, but the 90 GHz light curve at < 10 d is clearly severely under-predicted until 10 d. We find GRB 100418A inconsistent with the model, unless the excess is produced by a reverse shock that is hidden by forward shock emission at lower frequencies. The 90 GHz decline is slow for an RS, but may be transitioning from $\nu < \nu_m^{\text{RS}}$ to $\nu_m^{\text{RS}} < \nu$. [Laskar et al. \(2015\)](#) disfavored a reverse shock in this GRB, but did not explore it in detail. We note that, as in [Laskar et al. \(2015\)](#) and [Marshall et al. \(2011\)](#), our fit places the jet break at a much later time than the broken power law indicates.

3.18. GRB 111215A

A single pre-jet-break power law consistent with $p \approx 2.4$ and $\nu_c < \nu$ fits the X-ray data of this dark GRB until $t \sim 20$ d. Around this time, the 93 GHz light curve exhibits an unambiguous break if the upper limit at 41 d is considered. An X-ray break is not seen, but may have occurred around 20 d as well. The other radio light curves decay as single power laws consistent with ISM and $\nu_a < 4.9 \text{ GHz} < \nu_c < 19.1 \text{ GHz} < \nu_m < 93 \text{ GHz}$.

Based on the spectrum, $\max(\nu_m, \nu_a)$ seems to be located above 5 GHz until $\gtrsim 26$ d, perhaps as late as 45 d; while the light curve at 4.9 GHz already seems to decline at this point. A decline is, however, allowed if $\nu_a < \nu_m$ and the X-ray light curve breaks around the same time as the 93 GHz one. The 93 GHz break is roughly simultaneous with the peak at $\lesssim 20$ GHz and the end of X-ray observations, which also points toward an achromatic transition.

[Zauderer et al. \(2013\)](#) used the standard model with a jet break around the last X-ray observations; however, this does not provide a good fit to the late-time radio points. [van der Horst et al. \(2015\)](#) were able to fit the afterglow, placing a lower limit of > 31 d for the jet break. They, however, did not consider the effects of IC cooling (or emission), which is important with the ratio of $\epsilon_e/\epsilon_B \approx 2400$ of their best fit. Our model, which does include IC effects, can account for the X-ray and some of the radio light curve; however, our best ISM fit does not reproduce the 93 GHz light curve shape or the shape of the radio SED, while our wind fits, slightly better in terms of χ^2 , also cannot meet the upper limits at 1.4 d and ≤ 7 GHz. Thus we consider GRB 111215A inconsistent with our model.

3.19. GRB 140311A

The presence of an X-ray break is ambiguous ($P_F = 0.85$), but the X-ray light curve (Fig. 19) is consistent

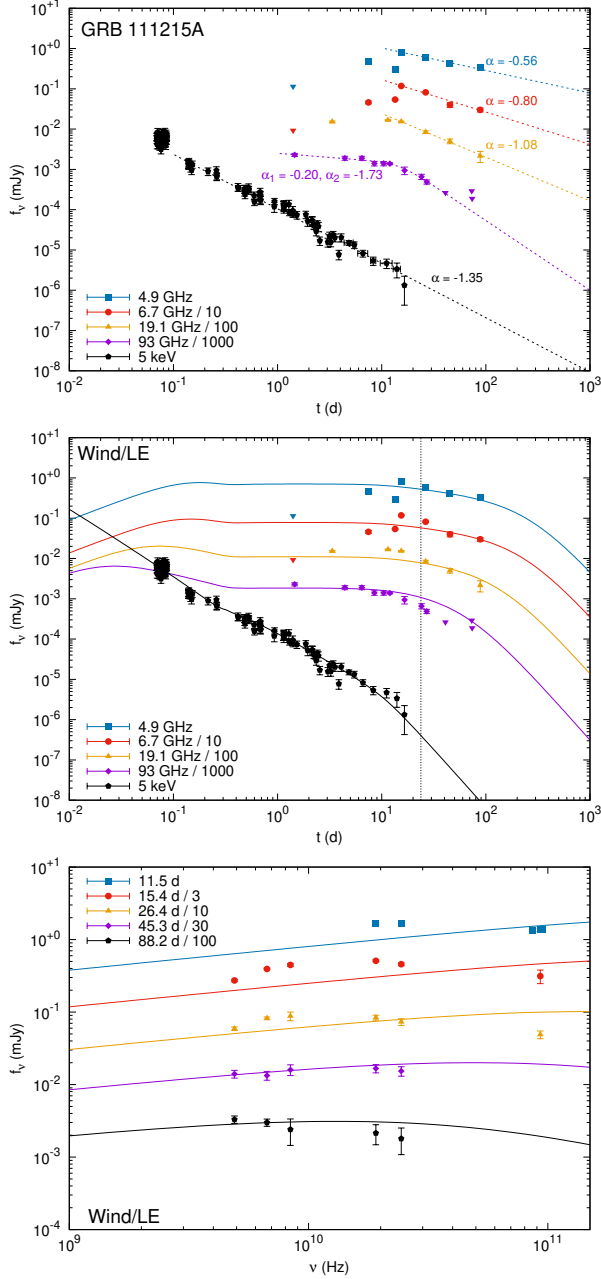


Figure 18. Our single and broken power law fits to the light curves of GRB 111215A (upper panel), and our best-fitting analytical model compared to the light curves (middle panel) and radio SEDs (lower panel). Four additional radio frequencies used in the fitting are omitted from the light curve figure for clarity.

with $p \approx 2.2$ and $\nu_c < \nu$; the large error on the post-break slope also makes it consistent with either lateral expansion or an edge effect. The radio light curves are mostly single power laws consistent with pre-break, $p \sim 2.1$ and $\nu_m < 8.6$ GHz; in this case we can set a limit of $t_{j,\text{radio}} \gtrsim 3t_{j,X}$. However, the light curve at ≤ 8.6

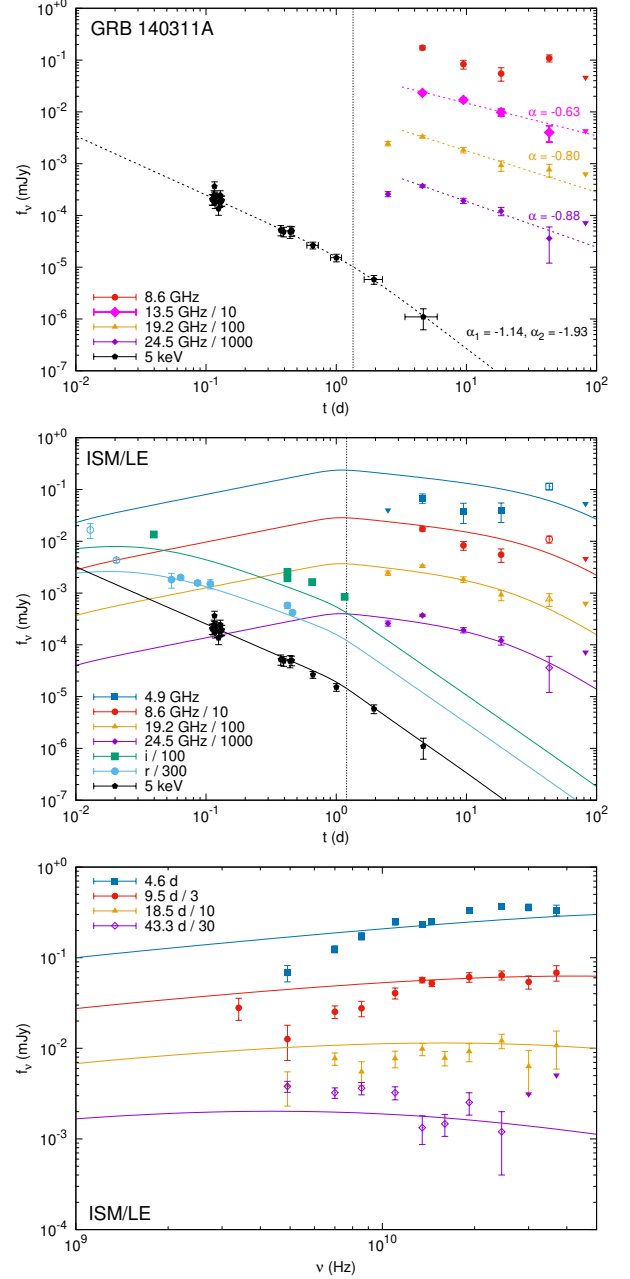


Figure 19. Our single and broken power law fits to the light curves of GRB 140311A (upper panel), and our best-fitting analytical model compared to the light curves (middle panel) and radio SEDs (lower panel). Nine additional optical and radio frequencies used in the fitting are omitted from the light curve figure for clarity.

GHz peaks again at ~ 40 d, which is at odds with the expected behavior and with other frequencies.

The SED indicates ν_m is located at $\gtrsim 25$ GHz when the 24.5 GHz light curve peaks (~ 5 d). However, the 8.6 and 13.5 GHz light curves also decline from this point on, while ν_m does not pass through 13.5 GHz until $\gtrsim 20$ d. A decline below ν_m is allowed by standard theory after

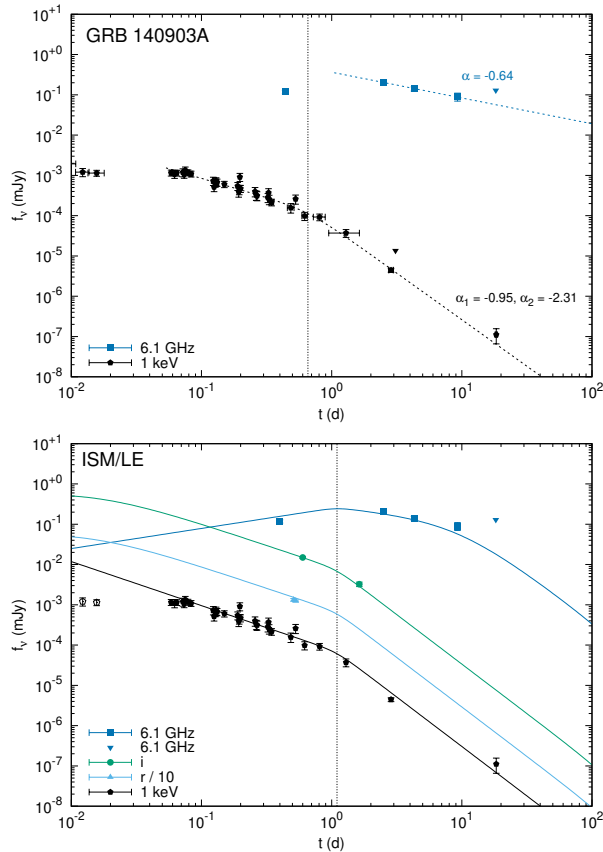


Figure 20. Our single and broken power law fits (upper panel) and best-fitting analytical model (lower panel) compared to the light curves of GRB 140903A.

the jet break, but in this case the slope of the light curve is steeper at all frequencies than the expected $-1/3$.

Our best-fit model is unable to reproduce the behavior of the radio SED, even when the late-time bump at 43 d is ignored. We also ignore the sharply declining optical feature at < 0.03 d. The optical, X-ray and $\gtrsim 10$ GHz light curves can be fitted reasonably well, but the model fails at the lowest observed frequencies ($\lesssim 9$ GHz). Laskar et al. (2018a) were able to fit the radio SED better (namely, their ν_a is located around 10 GHz), but cannot simultaneously fit the X-ray decline well. We can roughly reproduce their fit using their parameters. They consider the short-lived bump at ~ 40 d as possibly an early transition to a non-relativistic phase caused by a density enhancement. In summary, we consider GRB 140311A inconsistent with the standard model.

3.20. GRB 140903A

This short GRB is exceptional in its class in that it has an observed X-ray jet break (Troja et al. 2016). The X-ray light curve (Fig. 20) is consistent with $p \approx 2.3$

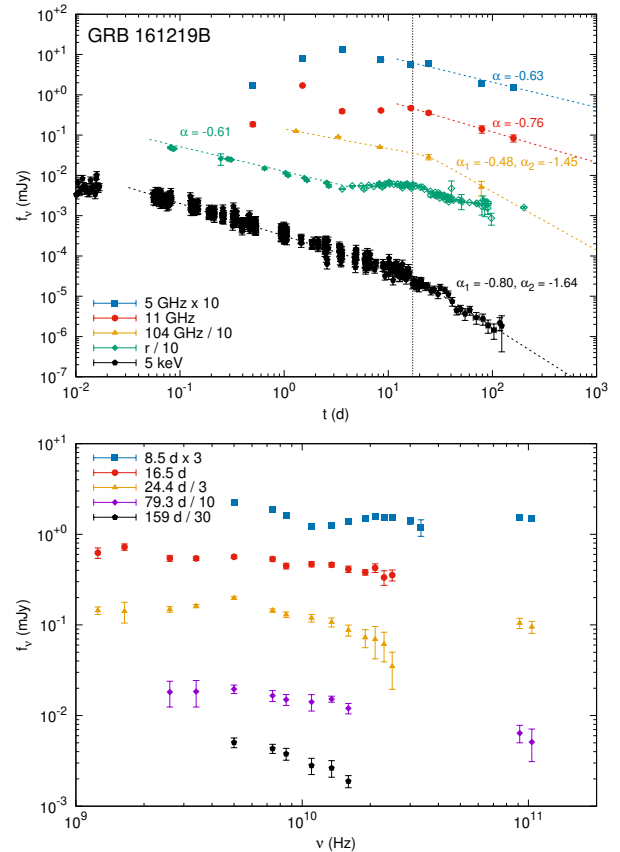


Figure 21. Our single and broken power law fits to the light curves of GRB 161219B (upper panel), and the evolution of the radio SED of this burst (lower panel).

and $\nu_m < \nu < \nu_c$ in an ISM-like CBM. However, the radio light curve at 6.1 GHz is inconsistent with this and would, instead, require a wind-type CBM (unlikely for short GRBs) and a fast-cooling spectrum ($\nu_m > \nu_c$) to be compatible with the standard model. We do note that the radio data are rather scarce for this burst.

Our best-fit model reproduces all light curves reasonably well, but the radio light curve does steepen around the last observed epoch. Troja et al. (2016) consider this burst as slightly off-axis. Even on-axis, their reported parameters, albeit not the best fit in terms of χ^2 , reproduce the data fairly well by eye. Thus we conclude that GRB 140903A remains consistent with the standard model.

3.21. GRB 161219B

The X-ray decline can be fitted with a broken power law, with a post-break slope of -1.64 ± 0.11 (Fig. 21). From the pre-break slope of -0.80 ± 0.01 one obtains $p \approx 1.7$, $\nu_c < \nu$; in which case an ISM-type CBM with either an edge-effect or lateral expansion break is a good match. The initial decline at 104 GHz is also consistent

with this using $p \approx 1.7$ and $\nu_m < 104 \text{ GHz} < \nu_c$. A value of p close to this ($p \approx 1.8$) also matches the r -band pre-jet-break decline of -0.61 ± 0.01 (we cannot fit the optical post-jet-break afterglow as it is dominated by SN2016jca and a late-time host galaxy contribution). However, the standard equations should not apply when $p < 2$. The Dai & Cheng (2001) equations, which should apply here, are not consistent with the early X-ray and optical slopes with any p between 1 and 2. Furthermore, the radio light curve (after the proposed reverse shock no longer dominates; Laskar et al. 2018b) at the frequencies with the longest follow-up settles onto a power law inconsistent with this scenario. If $\nu_X > \nu_c$, on the other hand, the early X-ray slope is consistent with $p \approx 2.1$, but the optical light curve is not. The 104 GHz curve seems to break at or after ~ 20 d; there are not enough post-break epochs for a proper broken power law fit, but simply using the last two points, one obtains a post-break slope of $\alpha_{2,104\text{GHz}} = -1.47 \pm 0.31$, consistent with the X-ray slope. A steeper slope is also possible if the break occurs later, though. This break is not seen at lower frequencies.

Our analytical model, being based on Granot & Sari (2002), is naturally unable to handle values of $p < 2$ that seem to be required by the optical and X-ray light curves. The model invoked by Laskar et al. (2018b) requires a refreshed reverse shock; however, even this model somewhat under-predicts the flux at late times, after their proposed jet break time. Additionally, Laskar et al. (2019) pointed out that the millimeter light curve of their model deviates somewhat from the observed light curve of this burst and of GRB 181201A. The spectrum does seem to require multiple peaks at least until 24.4 d, but the late-time spectra at ≥ 79.3 d are consistent with ν_m being located at ~ 5 GHz. All in all, the radio emission is inconsistent with the standard model, and only (roughly) consistent with the proposed refreshed reverse shock model shown in Laskar et al. (2018b) if the t^{-p} decline started soon after the last radio observations. Laskar et al. (2018b) also briefly bring up the possibility of either a host galaxy contribution to the late-time radio flux – which, however, is already included in said model – or an early transition to a non-relativistic phase, similarly to Laskar et al. (2018a).

4. DISCUSSION

4.1. Anomalous GRBs and jet break effects

As the jet break is a geometric effect, in standard GRB jet theory we should see a post-jet-break slope associated with it at all frequencies – even when the radio emission source is a population of thermal electrons behind the shock wave as suggested by e.g. Eichler & Waxman

(2005); Ressler & Laskar (2017); Warren et al. (2018). Several different power laws can be expected depending on the CBM profile, the presence of lateral expansion and the ordering of the break frequencies in the spectra (Rhoads 1999; Mészáros & Rees 1999; Granot & Sari 2002), as summarized in our Table 6. It is also possible to have a scenario where some lateral expansion is present, but the break is dominated by the edge effect (this was demonstrated in simulations by van Eerten & MacFadyen 2012). However, based on a large fraction of events of our sample, the situation may be more complicated in the radio.

In Table 7, we summarize how the radio light curve and SED evolve and whether they are consistent with the higher frequencies; we also describe how our analytical model fits the observations. For most of the GRBs in our sample, at late times we find a power-law decline in the radio whose slope is inconsistent with that expected based on the post-break X-ray or optical afterglow. In a few cases in our sample, we do see a post-jet-break radio slope predicted by the standard model and consistent with the same CBM type, spectral regime and p as the optical and X-ray; these are GRBs 090313 and 120326A in Group 1 and GRBs 000926 and 111215A in Group 2. More commonly, we see a decline consistent with *pre*-jet-break predictions until > 10 or even > 100 times later than the break seen in the X-rays or optical (namely, in GRBs 050820A, 110709B, 130907A, 160509A, 160625B and 171010A in Group 1 and GRBs 991208 and 000301C in Group 2), or inconsistent with all predicted slopes. As van Eerten et al. (2011) showed, break times may differ on different sides of ν_a and the break may broaden below ν_m , but in these simulations this effect was by a factor of a few, and in any case cannot explain the continuing *pre*-jet-break slope when the radio behavior is consistent with $\nu_m < \nu$. In six of the afterglows in our sample, with radio data both before and after the jet break, we see a simultaneous steepening of the radio light curve or at least cannot exclude it, indicating that the jet break does affect the radio (these are GRBs 990510, 050820A, 140903A, 160625B, 161219B and 171010A, while only GRBs 051022 and GRB 100418A do not show this), but the following decline is still generally inconsistent with predicted (asymptotic) power-law slopes. Furthermore, the radio light curves of eight GRBs (070125, 090313, 110709B, 130907A, 991208, 000301C, 000926 and 140311A) clearly continue rising after the X-ray jet break.

In the sample, we see one case where a $\sim t^{-2}$ decline is observed at ~ 10 GHz (GRB 120326A) and two others where it is seen at millimeter frequencies (GRBs 111215A and 161219B). The radio decline of

GRB	Radio behavior	Model fit
Group 1		
050820A	SPL consistent with pre-break until $\gtrsim 4t_{j,X}^a$	Consistent if very low density and opening angle
051022	SPL consistent with $\nu_m > 4.9$ GHz	Good
070125	SPL inconsistent with theory; late peak at low frequencies	Under-predicted 22.5 and 95 GHz light curves
090313	SPL consistent with $\nu_m > 16$ GHz, but too long	Over-predicted radio light curves; power law not reproduced
110709B	SPL consistent with pre-break until $> 60t_{j,X}$	Good
120326A	BPL	Under-predicted early X-ray light curve
130907A	SPL consistent with pre-break until $> 170t_{j,X}$	Under-predicted late radio light curves
141121A	Complex; multiple peaks	...
151027A	Hint of a break at ~ 100 d	Consistent if $p \approx 3.0$
160509A	SPL consistent with pre-break until $> 20t_{j,X}$	Good, but requires steepening after observations
160625B	SPL consistent with pre-break until $> 10t_{j,X}$	Over-predicted late 6.1 GHz light curves; power law not reproduced
171010A	SPL consistent with pre-break until $> 13t_{j,X}$; ν_m evolution too slow	Early radio spectrum not reproduced
Group 2		
990510	SPL inconsistent with theory	Good, but requires steepening after observations
991208	SPL consistent with pre-break until $\gtrsim 140t_{j,R}$	Fair
000301C	SPL consistent with pre-break until $\gtrsim 20t_{j,R}$	Under-predicted mm light curve; over-predicted early 4.9 and 8.5 GHz fluxes
000926	SPL consistent with post-break	Fair, but IC emission needed in X-rays
100418A	SPL inconsistent with theory; late peak at low frequencies	Under-predicted early mm light curve
111215A	BPL (93 GHz) or SPL consistent with post-break	Over-predicted early < 10 GHz light curves
140311A	SPL consistent with pre-break until late-time re-brightening; SED inconsistent with light curve	Over-predicted < 10 GHz light curves
140903A	SPL only consistent with $\nu_m > \nu_c$ until late times	Fair, but requires steepening after observations
161219B	BPL (~ 100 GHz) or SPL inconsistent with theory	...

^aThese limits are based on the last radio detection of each target.

Table 7. Summary of our main findings. For each GRB, we briefly describe the radio behavior based on our single and broken power law fits, and whether it is consistent with the X-ray behavior in some scenario of the standard jet model. We also describe whether the best-fit analytical model is a reasonable match with the observations.

GRB 120326A before the $\sim t^{-2}$ decline is seemingly inconsistent with expectations if the steepening corresponds to a post-jet-break passage of ν_m ; however, a smooth transition is able to reproduce the shape of the light curve (although the early X-ray fluxes are simultaneously under-predicted). The light curve scenarios described above and in K20, with a seemingly single power law inconsistent with any asymptotic power law in the standard model, can, therefore, at least in some cases simply be the result of an insufficiently long follow-up. In almost all cases, the constraints we have on the evolution of ν_m , based on the timing of its observed passage (including the aforementioned steepening in a millimeter light curve), are not strict enough to say a break onto a $\sim t^{-2}$ decline should have happened. This is not always the case, however: in GRBs 090313 and 130907A our code is unable to reconcile the lack of a $\sim t^{-2}$ decline with other frequencies. In four cases (GRBs 990510,

110709B, 140903A and 160509A), the model light curve is consistent with the data but steepens around the last observed radio point.

A caveat exists for the GRBs where the standard model cannot be excluded. Whether the single or broken power law of the radio decline is consistent with theoretical predictions is not an indicator of whether our code can find a reasonable fit for it. For example, GRB 111215A is found inconsistent with the standard model by our code despite the light curve slopes, while GRB 160509A is consistent with it. Smooth transitions between power law segments can account for some of the inconsistencies, while the GRBs with seemingly consistent slopes may be ruled out through other constraints. As per Table 7, no systematic difference is seen in the overall radio behavior of the GRBs consistent and inconsistent with the model.

As our Group 1 constitutes a representative sample, we can use it to study the fraction of the general (radio-loud) GRB population that is consistent with the standard model. Out of the 12 objects in Group 1, we find three (GRBs 051022, 110709B and 160509A) to be unambiguously consistent with the model, while two (GRBs 050820A and 151027A) are consistent with it if one allows unusual parameter ranges. Counting these two, we thus arrive at five events consistent with the model, out of 12; this means a fraction⁷ of $0.42^{+0.19}_{-0.17}$ for the well-fit afterglows out of all radio-loud GRBs. This number does not change when one checks the best fits for Klein-Nishina effects (Nakar et al. 2009); see Appendix B. This implies that in a significant fraction of GRBs, the physical parameters (e.g. CBM density and jet energy) determined through comparison to the standard model may be incorrect, in turn possibly affecting our understanding of the mechanism of the central engine. In the non-representative Group 2, we are able to fit four afterglows out of nine – these include two events in our sample that were included in Panaitescu & Kumar (2004), where their radio decline was considered anomalously shallow (GRBs 991208 and 000926). In both of these cases, a transition to the non-relativistic phase can explain the behavior. A non-relativistic transition was also suggested by Frail et al. (2004) to explain the late-time flattening they observed in some GRBs. While our modeling results indicate that flatness or shallowness of the radio decline is not *necessarily* a problem, it also suggests that non-relativistic transitions can not explain cases such as GRBs 160625B or 171010A.

4.2. Secondary emission component

One explanation for the long-lasting single power-law decline of the radio emission might be the presence of a wider jet surrounding a more energetic narrow core, which dominates in the radio (similar to that suggested by Berger et al. 2003). The greater width of this jet would produce a later break time than that expected from the narrower ‘main’ jet. Another separate source of radio-dominated emission could be the injection of energy into the reverse shock in the form of slower ejecta catching up to it, suggested by Sari & Mészáros (2000) and Panaitescu & Kumar (2004)⁸. However, if one of these scenarios applies to a GRB and the radio emission is dominated by a second source at a certain epoch, the

radio emission associated with the narrow jet must then be significantly weaker than the observed flux at that epoch.

To investigate the plausibility of producing faint radio emission from the narrow jet within the confines of the standard model, we have re-run our model-fitting code for the bursts in our sample with relatively good X-ray and optical coverage (GRBs 990510, 050820A, 070125, 090313, 120326A, 130907A, 140311A and 160625B)⁹. The fits were run *without radio data*, and at the last MCMC iteration, the parameters of each individual walker were used to create a light curve (as the fitting is run with 500 walkers, this means 500 light curves per burst). The resulting distribution of light curves at radio frequencies was then compared to the radio data. If this distribution includes light curves that significantly under-predict the observed radio fluxes at the corresponding epochs (disregarding the *shape* of the light curve), then the two-component scenario may be able to explain the light curve. If this is not the case, then an additional emission source would likely over-predict the radio fluxes. We include objects where the modeling code did not produce a good radio fit (GRBs 070125, 090313, 130907A, 140311A and 160625B), as this may have been due to the shape and peak time of the light curve instead of the general flux level. Two examples of the results of these tests are shown in Figure 22.

For GRB 990510, which is consistent with the standard model regardless of the CBM type, the wind fits are able to reach a factor of ~ 20 below the observed fluxes, while the ISM fits do so by a factor of ~ 2 . The radio fluxes of GRB 050820A are never significantly under-predicted in our ISM fits, but are under-predicted by a factor of > 10 in wind fits – the situation is very similar for GRB 140311A. Both of these seem to require an ISM-type CBM based on their optical and X-ray light curves, though. The radio fluxes of GRBs 090313 and 160625B are over-predicted in all of the test fits. On the other hand, the radio light curves of GRBs 070125 and 130907A are under-predicted in most test fits, and often stay below the observed flux level the entire time. This suggests that the two-component scenario may only be relevant for certain GRBs, or requires a mechanism to suppress the radio emission from the narrow jet; such a mechanism may be required in any case to produce radio quiet GRBs (Hancock et al. 2013; Lloyd-Ronning & Fryer 2017). However, the lack of radio quiet bursts with high E_{iso} would then also need to be explained.

⁷ Here, we have used Gehrels (1986) to determine the uncertainty of the fraction.

⁸ Laskar et al. (2018b) also suggest a reverse shock with energy injection for GRB 161219B, but not to explain the late-time radio light curve.

⁹ GRB 151027A was not included as, despite being tentatively consistent with the standard model, it is possible the X-ray is dominated by the late-prompt emission (Nappo et al. 2017).

Furthermore, in the two-component model one would naively expect to observe some GRBs whose radio emission clearly exceeds what the standard model predicts based on higher-frequency emission. We do, in fact, find one such object: GRB 130907A. We can only obtain a good fit to the X-ray and optical when ignoring the radio data, in which case the radio flux is under-predicted. This suggests that at least in the case of this particular GRB the scenario may very well be at work (as suggested by Veres et al. 2015), especially since its radio decline is consistent with pre-break when $p \approx 2$. However, as noted above, several of the afterglows seem to exhibit a steepening light curve simultaneously with the jet break, even if the following decline does not match asymptotic predictions. This argues against the presence of a secondary component, not associated with the forward shock of the main jet, dominating the radio emission at that time.

4.2.1. Reverse shock with energy injection

It is possible to further test the possibility of a reverse shock and late-time energy injection suggested by Panaitescu & Kumar (2004). This is, however, a toy model that does not capture the full behavior of a reverse shock and its light curve under energy injection. In this scenario, the fireball energy $E \propto t^e$ and the mass of ejecta energized by the reverse shock $M(> \Gamma) \propto \Gamma^{-q}$. The decline of the radio light curve of the reverse shock is

$$-\alpha_{\text{RS}} = \frac{3-e}{2} + \frac{6-k-e(2-k)}{4(4-k)}(p-1) - \frac{3-e-k}{2(4-k)}q. \quad (4)$$

To use this equation to obtain q , one must first find e using a higher frequency post-jet-break (forward shock) light curve. Without lateral expansion this is

$$-\alpha = \frac{3-e}{4}p - \frac{e(16-5k)-k}{4(4-k)} \quad (\nu < \nu_c) \quad (5)$$

or

$$-\alpha = \frac{3-e}{4}p - \frac{e(6-k)+k-2}{2(4-k)} \quad (\nu_c < \nu), \quad (6)$$

and with lateral expansion

$$-\alpha = p - \frac{p+2}{3}e. \quad (7)$$

These equations (based on Eqs. 42, 43 and 30 in Panaitescu & Kumar 2004) assume that $\nu_m(\text{RS}) < \nu_{\text{radio}}$. We also check for the possibility that $\nu_a(\text{RS}) < \nu_{\text{radio}} < \nu_m(\text{RS})$, in which case, from their Eq. 41, we can obtain

$$\alpha_{\text{RS}} = \frac{(3q-10)(3-e-k) - 2k(1+e)}{6(4-k)}. \quad (8)$$

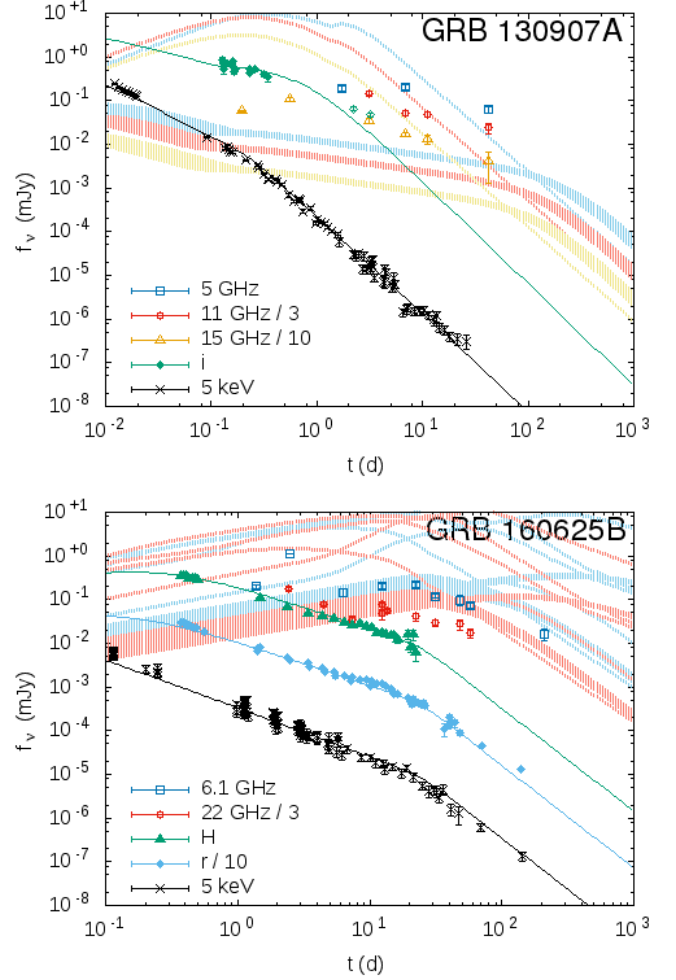


Figure 22. The best-fitting X-ray and optical light curves and the range of variation in radio light curves for 500 walkers in GRBs 130907A and 160625B, when fitting without radio data. The radio fluxes of GRB 130907A are clearly under-predicted apart from one outlying walker, while those of GRB 160625B are close to the observed fluxes. Thus GRB 130907A can have a dominant contribution from a secondary component without suppressing the flux from the narrow jet.

In this scenario, p must be determined using the spectrum.

We estimate e and q for those GRBs in our sample where this test is possible, i.e. when an X-ray spectral index (from the references in Table 1), a post-jet-break light curve and a radio power law fit are available, and where a secondary component was not deemed implausible in Section 4.2. The results are presented in Table 8. Problematic values are found for GRBs 051022 ($e < 0$ implies energy loss, not injection, in an adiabatic jet) and 160509A ($e \approx 0$ implies no injection). For GRB 130907A, the reverse shock and energy injection scenario

may be in effect if $\nu_{\text{radio}} < \nu_m(\text{RS})$ and $k = 2$, while in ISM scenarios $e < 0$.

4.3. Evolving microphysics

Some GRBs have been reported to require time-evolving microphysics (p , ϵ_e or ϵ_B); these include e.g. GRBs 091127 (Filgas et al. 2011) and 190114C (Misra et al. 2019). In these GRBs time-evolving ϵ_B and/or ϵ_e were required to explain, respectively, the anomalous evolution of ν_c and a discrepancy between α and β . A related issue was brought up by Gompertz et al. (2018), who noted numerous discrepancies between α and β requiring an intrinsic scatter of $\sigma_p \approx 0.25$ on values of p – one suggested cause was evolving microphysics. The functional dependence of these parameters on time is not well constrained by theory, but the evolution of break frequencies and the slope of the light curve are changed relative to the values in Table 6, possibly causing the light curve slopes seen in the sample. Signs of evolving microphysics could potentially be seen in some objects as, for example, a gradually changing X-ray photon index, which could be caused by an evolving p . GRB 130907A did exhibit a gradually rising X-ray photon index, but reached $\Gamma_X \approx 3.0$, which would require $p \approx 4$ if $\nu_m, \nu_c < \nu_X$; Margutti et al. (2015) ascribe this ‘super-soft’ X-ray spectrum instead to interaction with mass lost by the GRB progenitor. Such gradual Γ_X evolution is not seen in other bursts in our sample. Evolving ϵ_e or ϵ_B could, on the other hand, cause anomalous break frequency evolution – signs of this may be seen in GRB 171010A.

A proper investigation of this possibility is outside the scope of this paper, but we can briefly examine some examples. We use equations 3 and 5 in Misra et al. (2019) (based on Wijers & Galama 1999) and the fact that $f_\nu \propto f_m(\frac{\nu}{\nu_m})^{\frac{1}{2}}$ below ν_m and $f_\nu \propto f_m(\frac{\nu_c}{\nu_m})^{\frac{1-p}{2}}(\frac{\nu}{\nu_c})^{-\frac{p}{2}}$ above ν_c (assuming regime 1). We also assume, like them, that p remains constant, while $\epsilon_e \propto t^\lambda$ and $\epsilon_B \propto t^\lambda$. Then the pre-jet-break slope of the light curve below ν_m is $\alpha_{\text{ISM}} = \frac{1}{6}(2\lambda - 4\iota + 3)$ or $\alpha_{\text{wind}} = \frac{1}{6}(2\lambda - 4\iota)$. Above ν_c , we get $\alpha = \frac{1}{4}[p(\lambda - 3) + 2(1 - \lambda)] + \iota(p - 1)$. We now look at a few GRBs where the X-ray light curve suggests no lateral expansion, in which case the post-break slope changes by $-3/4$ in ISM or by $-1/2$ in wind. For GRB 171010A, the seemingly pre-break $t^{-1.1}$ radio light curve and the $t^{-2.0}$ X-ray light curve can both be reproduced if $p \approx 2.3$, $\iota \approx 0.1$ and $\lambda \approx -2.3$; for GRB 160509A we can similarly estimate $p \approx 2.2$, $\iota \approx 0$ and $\lambda \approx -1.9$, and for GRB 110709B, $p \approx 2.2$, $\iota \approx 0.3$ and $\lambda \approx -0.7$. As a comparison, Misra et al. (2019) obtain $\iota \approx -0.4$ and $\lambda \approx 0.1$ for GRB 190114C after a more robust analysis, while Filgas et al. (2011) suggest $\iota = 0$,

$\lambda = 0.49$ for GRB 091127. Thus there is a range of obtained parameters, both within this sample and between it and other results. Such variation does not rule out evolving microphysics, but does present another requirement for this potential solution.

4.4. Other considerations

It is noteworthy that some of the ‘well-behaving’ radio light curves (the aforementioned GRBs 990510, 050820A, 051022, and 110709B) may in fact be coincidental – in these cases we only have one radio frequency with enough points for power-law fitting, and some other GRBs in the sample exhibit a radio SED that our model fits cannot reproduce. As a cautionary example, GRB 070125 would appear consistent with the standard model if the 95 GHz data and late 22.5 GHz points were not observed. This means that one must remain careful in these cases. The same applies to the objects in Group 2 with no X-ray data. GRBs 051022, 110709B, 140903A and 160509A, all consistent with the model, also suffer from a lack of optical constraints. Out of the eight GRBs with good optical and X-ray coverage mentioned above, we find three that fit the standard model. Those bursts where the slope is consistent with pre-break expectations may also be inconsistent with them at other frequencies. A further complication is that, in some cases, the radio spectrum indicates that the decline compatible with $\nu_m < \nu$ sets in even before the ν_m passage, or the shape of the spectrum stays flat.

In addition to the two-component scenario mentioned above, other factors not included in our code can also have an effect on the light curve. A counter-jet was suggested as a way to explain the radio flux of GRB 980703 at ~ 1000 d by Perley et al. (2017), although the shape of the light curve is not conclusive. Counter-jets in general should peak roughly at $2(1+z)t_{NR}$, where t_{NR} is the beginning of the non-relativistic phase (Zhang & MacFadyen 2009), and at the peak their flux should be ~ 6 times the flux of the approaching jet. Most of our model fits place t_{NR} after the last radio observations; often absence of a non-relativistic transition in the X-ray light curve constrains t_{NR} to be late enough that the counter-jet cannot influence the radio light curve; and a late-time bump is usually not seen in the light curve. However, a counter-jet may conceivably be affecting GRB 070125.

Apart from a rough test for whether our best fits may be affected by the Klein-Nishina limit (Nakar et al. 2009), described in Appendix B, we have not included these effects in our code, as they are mostly ignored in GRB modeling efforts. These effects are not seen in the radio light curves, but a full inclusion of Klein-Nishina effects might result in some new sets of parameters be-

Table 8. Estimates of e and q parameters in the reverse shock and energy injection scenario.

GRB	$\nu_m(\text{RS}) < \nu_{\text{radio}}$	$\nu_{\text{radio}} < \nu_m(\text{RS})$
051022	$e \approx -0.4; q \approx 4.0$ (ISM) or $q \approx -0.8$ (wind)	$e \approx -0.4; q \approx 2.2$ (ISM) or $q \approx 2.6$ (wind)
070125	$e \approx 0.1, q \approx 3.6$	$e \approx 0.1, q \approx 1.7$
110709B	$e \approx 0.2, q \approx 3.6$	$e \approx 0.2, q \approx 1.3$
130907A	$e \approx -0.3, q \approx 3.6$ (ISM) or $e \approx 0.1, q \approx -2.7$ (wind)	$e \approx -0.3, q \approx 1.5$ (ISM) or $e \approx 0.14, q \approx 1.8$ (wind)
140903A	$e \approx 0.1, q \approx 3.7$	$e \approx 0.1, q \approx 1.6$
160509A	$e \approx 0, q \approx 2.8$	$e \approx 0, q \approx 0.9$

ing compatible with the X-ray data – parameters that our code now excludes.

We also note that in nine cases (italicized in Table 5) our code is unable to distinguish between a wind and an ISM density profile using the data available to us; both models result in almost equal χ^2 . Even for the other GRBs, unless only one of the models is consistent with the data (as with GRBs 050820A and 140903A), the other can typically not be excluded based on the model fits. Other observational signatures, such as the difference in light curve power laws above and below ν_m , can be used to make the distinction in some cases such as GRB 990510, where the light curve indices favor the ISM profile, but interestingly enough, the wind model results in a slightly better fit. In reality, the density profile may also not be as simple as is commonly assumed, particularly if eruptive mass loss dominates in the late stages of the star’s evolution.

Finally we point out that an object outside our sample, GRB 170817A, eventually exhibited a t^{-p} decline in the radio (Mooley et al. 2018; Lamb et al. 2019; Hajela et al. 2019). This particular afterglow requires a structured jet model with $p = 2.15^{+0.01}_{-0.02}$ and a relatively large observing angle of $30.4^{+4.0}_{-3.4}$ deg; because of the latter, the post-break decline was seen only when nearly non-relativistic. Its observation was made possible by a long follow-up, prompted by the gravitational waves and kilonova accompanying the event (e.g. Abbott et al. 2017; Kilpatrick et al. 2017; Tanvir et al. 2017). A structured jet is expected to delay and soften a jet break (Kumar & Granot 2003) and steepen the pre-break light curve (when the structure function is a power law; Panaitescu 2005). There should, however, be no steepening effect on post-break slopes. We also note that the objects in Panaitescu (2005) where the top-hat jet model did not fit the data well were not fit well by the structured jet model either, and the fit was not improved in 4 out of 10 cases.

5. CONCLUSIONS

We have examined a sample of 21 GRB afterglows with evidence of a jet break, but with otherwise varying properties. The sample is divided into two groups:

Group 1 consists of a representative sample of 12 GRBs from the *Swift* catalog, while Group 2 adds in 9 GRBs found through a literature search – these either predate *Swift* or do not match all of the search criteria. We have used both single/broken power law fits to the light curves and a fitting code based on the standard model (Mészáros & Rees 1999; Rhoads 1999; Sari & Esin 2001; Granot & Sari 2002; van der Horst 2007).

In most cases, while conventional fireball/jet theory can provide a good fit to the X-ray (and optical) light curve, it does a worse job with their radio light curves and/or SEDs. The decline of the radio light curve is mostly well described by a single power law inconsistent with predictions of the post-break decline. Sometimes (eight cases out of 21) the single power law is consistent with theoretical predictions for the *pre*-break decline, however, even up to several tens of times later than the jet break time.

According to our model fitting code, the standard model is able to account for the observed behavior of roughly half of all the examined GRBs, and a fraction of $0.42^{+0.19}_{-0.17}$ of the more representative Group 1. However, even in these cases the radio data mostly do not show a power-law decline consistent with post-break predictions. Even when the standard model fits the data anyway, in several cases it requires a steepening to $\sim t^{-2}$ soon after the last radio observations. Furthermore, three of these bursts have little to no optical data to constrain the fits. While GRB 120326A is an example of a GRB that eventually exhibited this steepening, the prediction highlights the importance of long radio follow-up of individual GRBs in order to confirm or exclude it. We also note that in many cases, the difference in χ^2 between ISM and wind models is very small, making it difficult to firmly establish the density profile using the available data.

All in all, in individual cases, the model fit in the radio may seem adequate, especially considering the typical errors and often small numbers of data points per band in the literature, but looking at a larger sample of events, a pattern emerges. A single power law fit to the radio, mostly inconsistent with asymptotic power law predictions, tends to describe the light curve at least as

well as model fits based on the standard jet model. We investigate the possibility of a secondary component (a wider jet or reverse shock emission with energy injection) dominating the late-time radio emission. This addition may explain a part of the anomalous afterglows, but in some cases requires another effect to suppress the emission from the forward shock of the narrow jet, and is disfavored in the cases where some light-curve steepening is seen simultaneously with the jet break. Evolving microphysics parameters may reproduce at least some of the observed post-jet-break light curves.

As Group 1 of our sample includes all GRBs in the *Swift* catalog with X-ray jet breaks and published radio data, it is both representative and contains GRBs with a range of properties. Thus the large fraction of objects whose behavior cannot be reproduced by our model fits, along with the scarcity of unambiguous cases of objects that behave as predicted by the standard model (and the lack of constraints associated with them), is telling. Along with the radio-quiet GRB population (Hancock et al. 2013; Lloyd-Ronning & Fryer 2017; Lloyd-Ronning et al. 2019), this highlights our lack of understanding of this part of the GRB afterglow spectrum and, quite possibly, the relevant physics. This problem may be better investigated in the future through radio and millimeter follow-up programs which continue until long after an observed X-ray or optical break. Until then,

the physical parameters determined for GRBs may contain systematic errors.

We thank the two anonymous referees for many comments and suggestions that prompted extensive changes to this paper, improving it considerably. We also thank Dale Frail, Alexander van der Horst, Asaf Pe'er and Chryssa Kouveliotou for helpful feedback and discussion.

Based on observations made with the NASA/ESA *Hubble Space Telescope* (programme GO 14353, PI Fruchter), obtained through the data archive at the Space Telescope Science Institute (STScI). STScI is operated by the Association of Universities for Research in Astronomy, Inc. under NASA contract NAS 5-26555. Support for this work was also provided by the National Aeronautics and Space Administration through Chandra Award Number 17500753, PI Fruchter, issued by the Chandra X-ray Center, which is operated by the Smithsonian Astrophysical Observatory for and on behalf of the National Aeronautics Space Administration under contract NAS8-03060. This work made use of data supplied by the UK Swift Science Data Centre at the University of Leicester.

APPENDIX

A. LATERAL EXPANSION AND NON-RELATIVISTIC PHASE BELOW ν_{ac}

Below ν_{ac} , the behavior of the light curve is given in Granot & Sari (2002) for the pre-break and edge-effect break cases. However, the source of most of the light curve power-law segments in the cases of lateral expansion and non-relativistic phase, van der Horst (2007), ignores ν_{ac} entirely. Thus, for completeness, we use Eq. 5 in Granot et al. (2000) to get

$$\nu_{ac}(t) = \left(\frac{6m_e^{12} c^{29} \Gamma^5 n'^{11}}{\pi^5 \epsilon_B^2 \epsilon_e^8 q_e^4 e'^{10}} \right)^{1/5} \propto \left(\frac{\Gamma(t)^5 n'(t)^{11}}{e'(t)^{10}} \right)^{1/5}, \quad (\text{A1})$$

where $\Gamma(t) \propto t^{-1/2}$ in the jet-spreading phase and $\Gamma(t) \approx 1$ in the non-relativistic phase; $n'(t) \propto \Gamma(t)n(t)$ and $e'(t) \propto \Gamma(t)^2 n(t)$. Therefore in the jet spreading phase, where the jet radius $R \approx \text{const}$ (e.g. Kumar & Zhang 2015), we obtain $\nu_{ac} \propto \Gamma(t)^{-4/5} \propto t^{4/10}$ in both ISM and wind cases. From

$$F_\nu(\nu < \nu_{ac} < \nu_a < \nu_c < \nu_m) = F_{\nu, \max} \left(\frac{\nu_a}{\nu_c} \right)^{1/3} \left(\frac{\nu_{ac}}{\nu_a} \right)^{11/8} \left(\frac{\nu}{\nu_{ac}} \right)^2, \quad (\text{A2})$$

$$F_\nu(\nu_{ac} < \nu < \nu_a < \nu_c < \nu_m) = F_{\nu, \max} \left(\frac{\nu_a}{\nu_c} \right)^{1/3} \left(\frac{\nu}{\nu_a} \right)^{11/8} \quad (\text{A3})$$

and using Table 2.10 of van der Horst (2007) for the behavior of $F_{\nu, \max}$, ν_c and ν_a , we obtain $F_\nu(\nu < \nu_{ac} < \nu_a < \nu_c < \nu_m) \propto t^0$ and $F_\nu(\nu_{ac} < \nu < \nu_a < \nu_c < \nu_m) \propto t^{1/4}$. In the non-relativistic phase and with ISM-type CBM, both Γ and n are roughly constant and hence $\nu_{ac} \propto t^0$. From Eqs. A2 and A3 and Table 2.11 of van der Horst (2007) it then follows that both $F_\nu(\nu < \nu_{ac} < \nu_a < \nu_c < \nu_m)$ and $F_\nu(\nu_{ac} < \nu < \nu_a < \nu_c < \nu_m)$ evolve as $t^{7/8}$. In a wind-type CBM, we have $n(t) \propto R(t)^{-2} \propto t^{-4/3}$, and thus, $\nu_{ac} \propto t^{-4/15}$. Using the same table, we thus obtain $F_\nu(\nu < \nu_{ac} < \nu_a < \nu_c < \nu_m) \propto t^{-121/72}$ and $F_\nu(\nu_{ac} < \nu < \nu_a < \nu_c < \nu_m) \propto t^{-133/72}$.

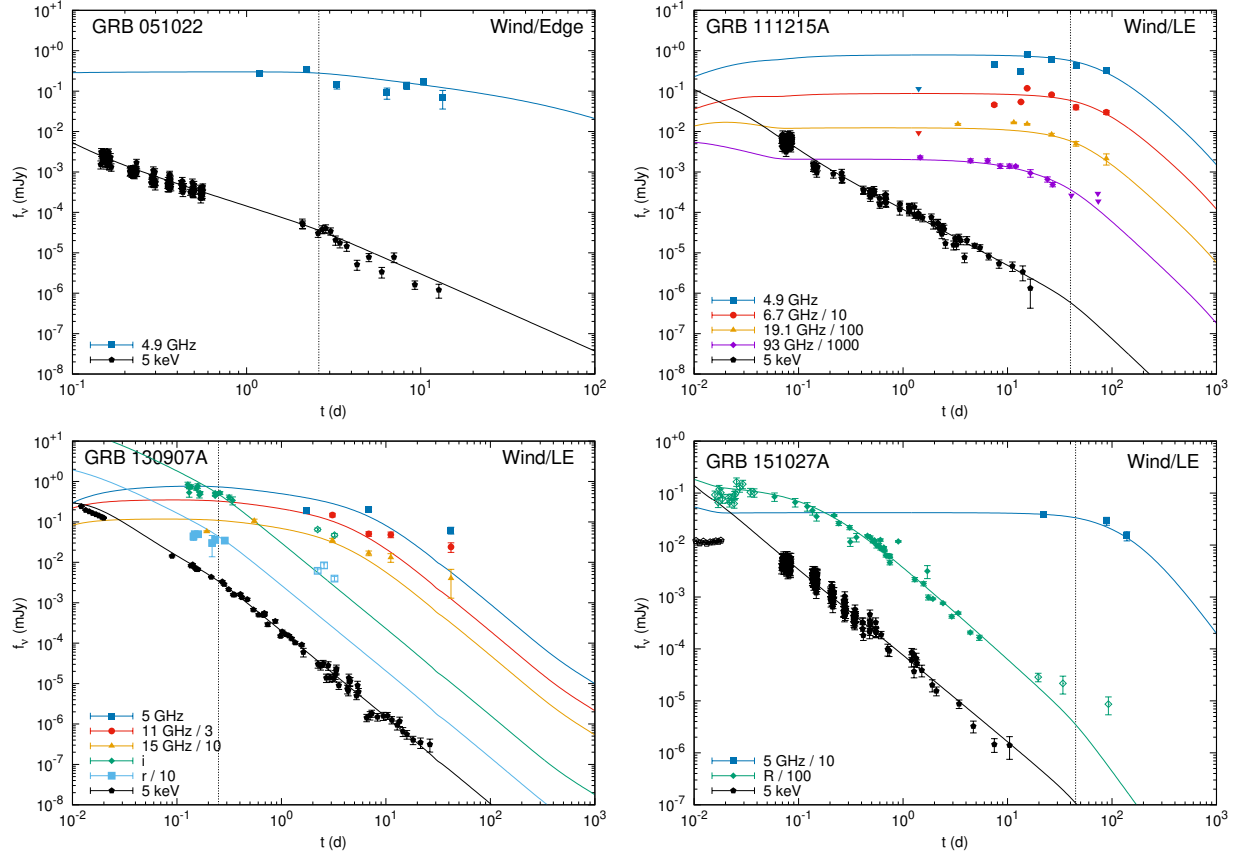


Figure 23. The best fits from the test for Klein-Nishina effects, run with a limitation on the maximum value of the Y parameter from Eq. A1.

B. THE POSSIBILITY OF KLEIN-NISHINA EFFECTS

As in some cases our modeling code predicts that IC effects (Sari & Esin 2001) are important, we also test whether the best-fit model of each afterglow is affected by Klein-Nishina (KN) effects (Nakar et al. 2009). As the energies of photons become comparable to the electron rest mass at the KN limit, the scattering cross section changes and electron cooling is slowed, hardening the spectrum at high energies ($\nu > \nu_c$); this can happen in some GRB afterglows, but most afterglows are only expected to be weakly affected.

Our code, based on the standard afterglow theory widely used by the GRB community, does not include the full analytical treatment of KN effects on the spectrum as described in Nakar et al. (2009). However, we can test each best-fit model for significant KN suppression of IC cooling. This is done using their Eq. 64 for the maximum value of the Y parameter:

$$Y_{max}(\gamma_c) \approx 10e^{\frac{27(3.2-p)^2-17}{(p+2)(4-p)}} \epsilon_{e,-1}^{\frac{5(p-1)}{p+2}} E_{53}^{1/2} n^{\frac{s-p}{2(p+2)}} t_d^{-\frac{5(p-2)}{2(p+2)}}. \quad (\text{B4})$$

This equation can be used directly for ISM-type CBM, but in the wind case the density of the medium the shock moves into evolves as $n(t) = (3 \times 10^{35} \text{ cm}^{-1}) A_* R^{-2}$, the radius as $R \approx 2ct\Gamma^2$ and the bulk Lorentz factor as $\Gamma \approx (1/\theta_j)(t/t_j)^{-1/4}$ (c.f. Kumar & Zhang 2015). If $Y_{max}(\gamma_c)$ at $t = 1$ d is below the value of Y in regime 5 (i.e. the highest Y predicted by the model), and the IC-corrected ν_c is below the highest observed frequency, we conclude that KN effects are affecting the best fit.

In most cases, we find $Y_{max}(\gamma_c, 1 \text{ d}) \gg Y$, or a ν_c too high to have been observed, and the best fit is therefore unaffected. However, this is not the case for GRBs 051022, 111215A, 130907A and 151027A. For these GRBs, as a rough approximation, we have run a version of our code that incorporates the constraint $Y(t) \leq Y_{max}(\gamma_c, t)$, and assume that KN effects on IC emission are confined to higher frequencies than observed. As a result of this, the quality of the best fit remains similar in all cases except GRB 130907A, where the fit at X-rays is improved but the

GRB	Model	$E_{K,iso}$ (10^{52} erg)	p	n_0 (cm^{-3}) or A_*	ϵ_e	ϵ_B	θ_j (rad)	A_V (mag)
051022	Wind/Edge	$13.4^{+8.2}_{-3.4}$	$2.37^{+0.11}_{-0.06}$	$0.10^{+0.10}_{-0.06}$	$0.21^{+0.04}_{-0.05}$	$1.9^{+13.5}_{-1.6} \times 10^{-3}$	$0.06^{+0.02}_{-0.01}$... ^a
111215A	Wind/LE	219^{+22}_{-23}	2.45 ± 0.02	0.12 ± 0.02	0.06 ± 0.01	0.02 ± 0.01	0.06 ± 0.01	...
130907A	Wind/LE	421^{+77}_{-55}	2.12 ± 0.01	$0.31^{+0.05}_{-0.04}$	0.17 ± 0.02	$6.9^{+2.4}_{-1.6} \times 10^{-5}$	0.02 ± 0.01	1.3^b
151027A	Wind/LE	125^{+41}_{-50}	$2.78^{+0.02}_{-0.03}$	$5.6^{+9.3}_{-2.4} \times 10^{-3}$	$0.04^{+0.03}_{-0.01}$	$0.31^{+0.38}_{-0.23}$	$0.03^{+0.03}_{-0.01}$	0.5 ± 0.1

^aFor dark GRBs (GRBs 051022 and 111215A), optical extinction is not relevant and was fixed at zero.

^bFor GRB 130907A, extinction was fixed at $A_V = 1.3$ as per Veres et al. (2015) (see text).

Table 9. MCMC fit parameters and their uncertainties for each GRB tested for KN effects, assuming $Y(t) \leq Y_{max}(\gamma_c, t)$.

radio behavior is still unaccounted for. Our conclusions therefore do not change. The resulting parameters of these fits are given in Table 9 and the best-fit light curves presented in Figure 23.

REFERENCES

- Abbott, B. P., Abbott, R., Abbott, T. D., et al. 2017, *Physical Review Letters*, 119, 161101, doi: [10.1103/PhysRevLett.119.161101](https://doi.org/10.1103/PhysRevLett.119.161101)
- Alexander, K. D., Laskar, T., Berger, E., et al. 2017, *ApJ*, 848, 69, doi: [10.3847/1538-4357/aa8a76](https://doi.org/10.3847/1538-4357/aa8a76)
- Bennett, C. L., Larson, D., Weiland, J. L., & Hinshaw, G. 2014, *ApJ*, 794, 135, doi: [10.1088/0004-637X/794/2/135](https://doi.org/10.1088/0004-637X/794/2/135)
- Berger, E., Sari, R., Frail, D. A., et al. 2000, *ApJ*, 545, 56, doi: [10.1086/317814](https://doi.org/10.1086/317814)
- Berger, E., Kulkarni, S. R., Pooley, G., et al. 2003, *Nature*, 426, 154, doi: [10.1038/nature01998](https://doi.org/10.1038/nature01998)
- Beuermann, K., Hessman, F. V., Reinsch, K., et al. 1999, *A&A*, 352, L26. <https://arxiv.org/abs/astro-ph/9909043>
- Bloom, J. S., Kulkarni, S. R., Djorgovski, S., et al. 1999, *GRB Coordinates Network*, 323, 1
- Bright, J. S., Horesh, A., van der Horst, A. J., et al. 2019, arXiv e-prints. <https://arxiv.org/abs/1904.00039>
- Burns, E. 2016, *GRB Coordinates Network*, 19587, 1
- Cardelli, J. A., Clayton, G. C., & Mathis, J. S. 1989, *ApJ*, 345, 245, doi: [10.1086/167900](https://doi.org/10.1086/167900)
- Castro-Tirado, A. J., Sokolov, V. V., Gorosabel, J., et al. 2001, *A&A*, 370, 398, doi: [10.1051/0004-6361/20010247](https://doi.org/10.1051/0004-6361/20010247)
- Cenko, S. B., Kasliwal, M., Harrison, F. A., et al. 2006, *ApJ*, 652, 490, doi: [10.1086/508149](https://doi.org/10.1086/508149)
- Cenko, S. B., Frail, D. A., Harrison, F. A., et al. 2010, *ApJ*, 711, 641, doi: [10.1088/0004-637X/711/2/641](https://doi.org/10.1088/0004-637X/711/2/641)
- Chandra, P., Cenko, S. B., Frail, D. A., et al. 2008, *ApJ*, 683, 924, doi: [10.1086/589807](https://doi.org/10.1086/589807)
- Chiaberge, M., & Marconi, A. 2011, *MNRAS*, 416, 917, doi: [10.1111/j.1365-2966.2011.19079.x](https://doi.org/10.1111/j.1365-2966.2011.19079.x)
- Cucchiara, A., Veres, P., Corsi, A., et al. 2015, *ApJ*, 812, 122, doi: [10.1088/0004-637X/812/2/122](https://doi.org/10.1088/0004-637X/812/2/122)
- Dai, Z. G., & Cheng, K. S. 2001, *ApJL*, 558, L109, doi: [10.1086/323566](https://doi.org/10.1086/323566)
- De Pasquale, M., Page, M. J., Kann, D. A., et al. 2016, *MNRAS*, 462, 1111, doi: [10.1093/mnras/stw1704](https://doi.org/10.1093/mnras/stw1704)
- de Ugarte Postigo, A., Thöne, C. C., Bensch, K., et al. 2018, *A&A*, 620, A190, doi: [10.1051/0004-6361/201833636](https://doi.org/10.1051/0004-6361/201833636)
- Eichler, D., & Waxman, E. 2005, *ApJ*, 627, 861, doi: [10.1086/430596](https://doi.org/10.1086/430596)
- Filgas, R., Greiner, J., Schady, P., et al. 2011, *A&A*, 535, A57, doi: [10.1051/0004-6361/201117695](https://doi.org/10.1051/0004-6361/201117695)
- Foreman-Mackey, D., Hogg, D. W., Lang, D., & Goodman, J. 2013, *PASP*, 125, 306, doi: [10.1086/670067](https://doi.org/10.1086/670067)
- Frail, D. A., Metzger, B. D., Berger, E., Kulkarni, S. R., & Yost, S. A. 2004, *ApJ*, 600, 828, doi: [10.1086/380108](https://doi.org/10.1086/380108)
- Galama, T. J., Frail, D. A., Sari, R., et al. 2003, *ApJ*, 585, 899, doi: [10.1086/346083](https://doi.org/10.1086/346083)
- Galama, T. J., Bremer, M., Bertoldi, F., et al. 2000, *ApJL*, 541, L45, doi: [10.1086/312904](https://doi.org/10.1086/312904)
- Gehrels, N. 1986, *ApJ*, 303, 336, doi: [10.1086/164079](https://doi.org/10.1086/164079)
- Giannios, D., & Spitkovsky, A. 2009, *MNRAS*, 400, 330, doi: [10.1111/j.1365-2966.2009.15454.x](https://doi.org/10.1111/j.1365-2966.2009.15454.x)
- Golenetskii, S., Aptekar, R., Mazets, E., et al. 2005, *GRB Coordinates Network*, 4150, 1
- . 2007, *GRB Coordinates Network*, 6049, 1
- Golenetskii, S., Aptekar, R., Frederiks, D., et al. 2014, *GRB Coordinates Network*, 17108, 1
- Gompertz, B. P., Fruchter, A. S., & Pe'er, A. 2018, ArXiv e-prints. <https://arxiv.org/abs/1802.07730>
- Granot, J., & Piran, T. 2012, *MNRAS*, 421, 570, doi: [10.1111/j.1365-2966.2011.20335.x](https://doi.org/10.1111/j.1365-2966.2011.20335.x)
- Granot, J., Piran, T., & Sari, R. 1999a, *ApJ*, 513, 679, doi: [10.1086/306884](https://doi.org/10.1086/306884)
- . 1999b, *ApJ*, 527, 236, doi: [10.1086/308052](https://doi.org/10.1086/308052)
- . 2000, *ApJL*, 534, L163, doi: [10.1086/312661](https://doi.org/10.1086/312661)
- Granot, J., & Sari, R. 2002, *ApJ*, 568, 820, doi: [10.1086/338966](https://doi.org/10.1086/338966)

- Hajela, A., Margutti, R., Alexander, K. D., et al. 2019, arXiv e-prints, arXiv:1909.06393.
<https://arxiv.org/abs/1909.06393>
- Hancock, P. J., Gaensler, B. M., & Murphy, T. 2013, ApJ, 776, 106, doi: [10.1088/0004-637X/776/2/106](https://doi.org/10.1088/0004-637X/776/2/106)
- Harrison, F. A., Bloom, J. S., Frail, D. A., et al. 1999, ApJL, 523, L121, doi: [10.1086/312282](https://doi.org/10.1086/312282)
- Harrison, F. A., Yost, S. A., Sari, R., et al. 2001, ApJ, 559, 123, doi: [10.1086/322368](https://doi.org/10.1086/322368)
- Hurley, K., Mazets, E., Golenetskii, S., & Cline, T. 2000a, GRB Coordinates Network, 801, 1
- Hurley, K., Cline, T., Mazets, E., et al. 2000b, ApJL, 534, L23, doi: [10.1086/312645](https://doi.org/10.1086/312645)
- Israel, G. L., Marconi, G., Covino, S., et al. 1999, A&A, 348, L5. <https://arxiv.org/abs/astro-ph/9906409>
- Jensen, B. L., Fynbo, J. U., Gorosabel, J., et al. 2001, A&A, 370, 909, doi: [10.1051/0004-6361:20010291](https://doi.org/10.1051/0004-6361:20010291)
- Kangas, T., Fruchter, A. S., Cenko, S. B., et al. 2020, ApJ, 894, 43, doi: [10.3847/1538-4357/ab8799](https://doi.org/10.3847/1538-4357/ab8799)
- Kilpatrick, C. D., Foley, R. J., Kasen, D., et al. 2017, Science, 358, 1583, doi: [10.1126/science.aag0073](https://doi.org/10.1126/science.aag0073)
- Kippen, R. M. 1999, GRB Coordinates Network, 322, 1
- Kumar, P., & Granot, J. 2003, ApJ, 591, 1075, doi: [10.1086/375186](https://doi.org/10.1086/375186)
- Kumar, P., & Zhang, B. 2015, PhR, 561, 1, doi: [10.1016/j.physrep.2014.09.008](https://doi.org/10.1016/j.physrep.2014.09.008)
- Kuulkers, E., Antonelli, L. A., Kuiper, L., et al. 2000, ApJ, 538, 638, doi: [10.1086/309159](https://doi.org/10.1086/309159)
- Lamb, G. P., Lyman, J. D., Levan, A. J., et al. 2019, ApJ, 870, L15, doi: [10.3847/2041-8213/aaf96b](https://doi.org/10.3847/2041-8213/aaf96b)
- Laskar, T., Berger, E., Chornock, R., et al. 2018a, ApJ, 858, 65, doi: [10.3847/1538-4357/aab8f5](https://doi.org/10.3847/1538-4357/aab8f5)
- Laskar, T., Berger, E., Margutti, R., et al. 2015, ApJ, 814, 1, doi: [10.1088/0004-637X/814/1/1](https://doi.org/10.1088/0004-637X/814/1/1)
- Laskar, T., Berger, E., Tanvir, N., et al. 2014, ApJ, 781, 1, doi: [10.1088/0004-637X/781/1/1](https://doi.org/10.1088/0004-637X/781/1/1)
- Laskar, T., Alexander, K. D., Berger, E., et al. 2016, ApJ, 833, 88, doi: [10.3847/1538-4357/833/1/88](https://doi.org/10.3847/1538-4357/833/1/88)
- . 2018b, ApJ, 862, 94, doi: [10.3847/1538-4357/aacbcb](https://doi.org/10.3847/1538-4357/aacbcb)
- Laskar, T., van Eerten, H., Schady, P., et al. 2019, ApJ, 884, 121, doi: [10.3847/1538-4357/ab40ce](https://doi.org/10.3847/1538-4357/ab40ce)
- Lazzati, D., & Begelman, M. C. 2005, ApJ, 629, 903, doi: [10.1086/430877](https://doi.org/10.1086/430877)
- Liang, E.-W., Zhang, B.-B., & Zhang, B. 2007, ApJ, 670, 565, doi: [10.1086/521870](https://doi.org/10.1086/521870)
- Lloyd-Ronning, N. M., & Fryer, C. L. 2017, MNRAS, 467, 3413, doi: [10.1093/mnras/stx313](https://doi.org/10.1093/mnras/stx313)
- Lloyd-Ronning, N. M., Gompertz, B., Pe'er, A., Dainotti, M., & Fruchter, A. 2019, ApJ, 871, 118, doi: [10.3847/1538-4357/aaf6ac](https://doi.org/10.3847/1538-4357/aaf6ac)
- Margutti, R., Guidorzi, C., Lazzati, D., et al. 2015, ApJ, 805, 159, doi: [10.1088/0004-637X/805/2/159](https://doi.org/10.1088/0004-637X/805/2/159)
- Marshall, F. E., Antonelli, L. A., Burrows, D. N., et al. 2011, ApJ, 727, 132, doi: [10.1088/0004-637X/727/2/132](https://doi.org/10.1088/0004-637X/727/2/132)
- Melandri, A., Kobayashi, S., Mundell, C. G., et al. 2010, ApJ, 723, 1331, doi: [10.1088/0004-637X/723/2/1331](https://doi.org/10.1088/0004-637X/723/2/1331)
- Mészáros, P., & Rees, M. J. 1999, MNRAS, 306, L39, doi: [10.1046/j.1365-8711.1999.02800.x](https://doi.org/10.1046/j.1365-8711.1999.02800.x)
- Misra, K., Resmi, L., Kann, D. A., et al. 2019, arXiv e-prints, arXiv:1911.09719.
<https://arxiv.org/abs/1911.09719>
- Moin, A., Chandra, P., Miller-Jones, J. C. A., et al. 2013, ApJ, 779, 105, doi: [10.1088/0004-637X/779/2/105](https://doi.org/10.1088/0004-637X/779/2/105)
- Mooley, K. P., Frail, D. A., Dobie, D., et al. 2018, ApJL, 868, L11, doi: [10.3847/2041-8213/aaeda7](https://doi.org/10.3847/2041-8213/aaeda7)
- Nakar, E., Ando, S., & Sari, R. 2009, ApJ, 703, 675, doi: [10.1088/0004-637X/703/1/675](https://doi.org/10.1088/0004-637X/703/1/675)
- Nappo, F., Pescalli, A., Oganessian, G., et al. 2017, A&A, 598, A23, doi: [10.1051/0004-6361/201628801](https://doi.org/10.1051/0004-6361/201628801)
- Oates, S. R., de Pasquale, M., Page, M. J., et al. 2007, MNRAS, 380, 270, doi: [10.1111/j.1365-2966.2007.12054.x](https://doi.org/10.1111/j.1365-2966.2007.12054.x)
- Paczynski, B., & Rhoads, J. E. 1993, ApJL, 418, L5, doi: [10.1086/187102](https://doi.org/10.1086/187102)
- Panaitescu, A. 2005, MNRAS, 363, 1409, doi: [10.1111/j.1365-2966.2005.09532.x](https://doi.org/10.1111/j.1365-2966.2005.09532.x)
- Panaitescu, A., & Kumar, P. 2001, ApJ, 554, 667, doi: [10.1086/321388](https://doi.org/10.1086/321388)
- . 2002, ApJ, 571, 779, doi: [10.1086/340094](https://doi.org/10.1086/340094)
- . 2004, MNRAS, 350, 213, doi: [10.1111/j.1365-2966.2004.07635.x](https://doi.org/10.1111/j.1365-2966.2004.07635.x)
- Panaitescu, A., & Mészáros, P. 1999, ApJ, 526, 707, doi: [10.1086/308005](https://doi.org/10.1086/308005)
- Pei, Y. C. 1992, ApJ, 395, 130, doi: [10.1086/171637](https://doi.org/10.1086/171637)
- Peng, F., Königl, A., & Granot, J. 2005, ApJ, 626, 966, doi: [10.1086/430045](https://doi.org/10.1086/430045)
- Perley, D. A., Hjorth, J., Tanvir, N. R., & Perley, R. A. 2017, MNRAS, 465, 970, doi: [10.1093/mnras/stw2789](https://doi.org/10.1093/mnras/stw2789)
- Perley, D. A., Cenko, S. B., Corsi, A., et al. 2014, ApJ, 781, 37, doi: [10.1088/0004-637X/781/1/37](https://doi.org/10.1088/0004-637X/781/1/37)
- Pietrzynski, G., & Udalski, A. 1999, IAUC, 7164, 2
- Piran, T. 2004, Reviews of Modern Physics, 76, 1143, doi: [10.1103/RevModPhys.76.1143](https://doi.org/10.1103/RevModPhys.76.1143)
- Poolakkil, S., & Meegan, C. 2017, GRB Coordinates Network, 21992, 1
- Price, P. A., Harrison, F. A., Galama, T. J., et al. 2001, ApJL, 549, L7, doi: [10.1086/319152](https://doi.org/10.1086/319152)
- Ressler, S. M., & Laskar, T. 2017, ApJ, 845, 150, doi: [10.3847/1538-4357/aa8268](https://doi.org/10.3847/1538-4357/aa8268)
- Rhoads, J. E. 1999, ApJ, 525, 737, doi: [10.1086/307907](https://doi.org/10.1086/307907)

- Rhoads, J. E., & Fruchter, A. S. 2001, *ApJ*, 546, 117, doi: [10.1086/318246](https://doi.org/10.1086/318246)
- Roberts, O. J., Fitzpatrick, G., & Veres, P. 2016, *GRB Coordinates Network*, 19411, 1
- Rol, E., van der Horst, A., Wiersema, K., et al. 2007, *ApJ*, 669, 1098, doi: [10.1086/521336](https://doi.org/10.1086/521336)
- Sagar, R., Mohan, V., Pandey, S. B., et al. 2000, *Bulletin of the Astronomical Society of India*, 28, 499. <https://arxiv.org/abs/astro-ph/0004223>
- Sari, R., & Esin, A. A. 2001, *ApJ*, 548, 787, doi: [10.1086/319003](https://doi.org/10.1086/319003)
- Sari, R., & Mészáros, P. 2000, *ApJL*, 535, L33, doi: [10.1086/312689](https://doi.org/10.1086/312689)
- Sari, R., Piran, T., & Halpern, J. P. 1999, *ApJL*, 519, L17, doi: [10.1086/312109](https://doi.org/10.1086/312109)
- Sari, R., Piran, T., & Narayan, R. 1998, *ApJL*, 497, L17, doi: [10.1086/311269](https://doi.org/10.1086/311269)
- Schlafly, E. F., & Finkbeiner, D. P. 2011, *ApJ*, 737, 103, doi: [10.1088/0004-637X/737/2/103](https://doi.org/10.1088/0004-637X/737/2/103)
- Smith, D. A. 2000, *GRB Coordinates Network*, 568, 1
- Stanek, K. Z., Garnavich, P. M., Kaluzny, J., Pych, W., & Thompson, I. 1999, *ApJL*, 522, L39, doi: [10.1086/312219](https://doi.org/10.1086/312219)
- Tanvir, N. R., Levan, A. J., González-Fernández, C., et al. 2017, *ApJL*, 848, L27, doi: [10.3847/2041-8213/aa90b6](https://doi.org/10.3847/2041-8213/aa90b6)
- Troja, E., Sakamoto, T., Cenko, S. B., et al. 2016, *ApJ*, 827, 102, doi: [10.3847/0004-637X/827/2/102](https://doi.org/10.3847/0004-637X/827/2/102)
- Troja, E., Lipunov, V. M., Mundell, C. G., et al. 2017, *Nature*, 547, 425, doi: [10.1038/nature23289](https://doi.org/10.1038/nature23289)
- Uhm, Z. L., & Beloborodov, A. M. 2007, *ApJL*, 665, L93, doi: [10.1086/519837](https://doi.org/10.1086/519837)
- van der Horst, A. J. 2007, PhD thesis, University of Amsterdam
- van der Horst, A. J., Levan, A. J., Pooley, G. G., et al. 2015, *MNRAS*, 446, 4116, doi: [10.1093/mnras/stu2407](https://doi.org/10.1093/mnras/stu2407)
- van Eerten, H., van der Horst, A., & MacFadyen, A. 2012, *ApJ*, 749, 44, doi: [10.1088/0004-637X/749/1/44](https://doi.org/10.1088/0004-637X/749/1/44)
- van Eerten, H. J., & MacFadyen, A. I. 2012, *ApJ*, 751, 155, doi: [10.1088/0004-637X/751/2/155](https://doi.org/10.1088/0004-637X/751/2/155)
- van Eerten, H. J., Meliani, Z., Wijers, R. A. M. J., & Keppens, R. 2011, *MNRAS*, 410, 2016, doi: [10.1111/j.1365-2966.2010.17582.x](https://doi.org/10.1111/j.1365-2966.2010.17582.x)
- Veres, P., Corsi, A., Frail, D. A., Cenko, S. B., & Perley, D. A. 2015, *ApJ*, 810, 31, doi: [10.1088/0004-637X/810/1/31](https://doi.org/10.1088/0004-637X/810/1/31)
- Warren, D. C., Barkov, M. V., Ito, H., Nagataki, S., & Laskar, T. 2018, *MNRAS*, 480, 4060, doi: [10.1093/mnras/sty2138](https://doi.org/10.1093/mnras/sty2138)
- Waxman, E., Kulkarni, S. R., & Frail, D. A. 1998, *ApJ*, 497, 288, doi: [10.1086/305467](https://doi.org/10.1086/305467)
- Wijers, R. A. M. J., & Galama, T. J. 1999, *ApJ*, 523, 177, doi: [10.1086/307705](https://doi.org/10.1086/307705)
- Xu, C., Livio, M., & Baum, S. 1999, *AJ*, 118, 1169, doi: [10.1086/301007](https://doi.org/10.1086/301007)
- Yost, S. A., Harrison, F. A., Sari, R., & Frail, D. A. 2003, *ApJ*, 597, 459, doi: [10.1086/378288](https://doi.org/10.1086/378288)
- Zauderer, B. A., Berger, E., Margutti, R., et al. 2013, *ApJ*, 767, 161, doi: [10.1088/0004-637X/767/2/161](https://doi.org/10.1088/0004-637X/767/2/161)
- Zhang, W., & MacFadyen, A. 2009, *ApJ*, 698, 1261, doi: [10.1088/0004-637X/698/2/1261](https://doi.org/10.1088/0004-637X/698/2/1261)